

## Spin-spin correlation functions for the square-lattice Heisenberg antiferromagnet at zero temperature

C. M. Canali

*Department of Physics, King's College London, Strand, London WC2R 2LS, United Kingdom*

Mats Wallin

*Department of Theoretical Physics, Royal Institute of Technology, 100 44 Stockholm, Sweden*

(Received 31 March 1993)

We have calculated the dynamical transverse and longitudinal spin-correlation functions for the two-dimensional Heisenberg antiferromagnet at zero temperature, by the Dyson-Maleev spin-wave theory to second order in perturbation theory. The transverse correlation function is characterized by a dominant one-magnon peak and a broad three-magnon continuum. For spin 1/2 the contribution of the three-magnon excitations is small but not negligible, and might be detected in highly sensitive neutron-scattering experiments in the undoped layered cuprates. We have also computed the transverse equal-time correlations and compared the results with recent series-expansion estimates. The good agreement between the two formalisms reinforces the validity of spin-wave theory. The longitudinal structure factor, to leading order, displays a two-peak structure similar to that obtained by the Schwinger-boson mean-field formalism. The magnon interaction reduces the second peak, in some cases substantially. We discuss how umklapp processes affect the multiple-magnon excitations. We have finally computed the staggered magnetization and transverse susceptibility corrected to second order. For spin 1/2 we find  $m = 0.3069 \pm 0.00020$  for the staggered magnetization, and  $Z_\chi = 0.4844 \pm 0.00010$  for the susceptibility renormalization constant, in agreement with the results obtained by other techniques.

### I. INTRODUCTION

The magnetic properties of the copper oxide planes of the high- $T_c$  materials in their insulating phase are believed to be correctly described by a square-lattice spin-1/2 Heisenberg antiferromagnet, with a rather large exchange constant,  $J$ , of order 1500 K.<sup>1</sup> This fact has fueled a renewed interest in the quantum Heisenberg antiferromagnet, of which very few exact results are known. Several analytical and numerical techniques have been developed over the years to study this problem. Among these, spin-wave theory (SWT), developed many years ago,<sup>2</sup> has proved to be a very useful and successful method. SWT provides accurate results for many physical quantities, even for the relevant and difficult case of the spin-1/2 Heisenberg antiferromagnet in two dimensions, where quantum fluctuations are strong. What is more surprising is that a renormalized version of the *linear* approximation of SWT is already in good quantitative agreement with more sophisticated numerical techniques.<sup>3,4</sup> All the calculated higher-order corrections to linear spin-wave theory (LSWT), in the expansion parameter  $1/S$ , are small but not negligible and further improve the LSWT results.<sup>5-9</sup> The only example which does not fit into this nice and consistent picture is the spin-pair excitation spectra, measured in Raman-scattering experiments in the insulating phase of the cuprate materials.<sup>10</sup> In this case the simplest SWT approximation, involving the scattering of two magnons,<sup>11</sup> gives a spectrum which does

not resemble the broad experimental line shape, with nonzero intensity up to 4 times the energy of one magnon. It was argued that this anomalous line shape is caused by strong quantum fluctuations present in the spin-1/2 system which, in the SWT picture, appear as multiple-magnon excitations overlapping and giving a large intensity at high frequencies. This hypothesis seemed to be confirmed by the calculation of the first three frequency moments of the spin-pair excitation spectra by series-expansion methods,<sup>12</sup> which were found to be rather close to the experimental results. A different conclusion came from a recent spin-wave study of the Raman line shape,<sup>13</sup> where it was shown that the most important correction to the intense and narrow two-magnon peak comes from four-magnon scattering, whose intensity is very small and well separated in energy from the dominant two-magnon contribution. Nevertheless, because of the large separation between the two- and four-magnon peaks, the first two frequency moments are in good agreement with the series-expansion estimates. In Ref. 13 it was suggested that this result could well mean that the model used so far in this problem is not correct. In particular, the effective coupling between light and the spin system is more complicated than a simple spin-pair Hamiltonian because of strong resonance effects, involving real charge-transfer excitations,<sup>14</sup> which make it difficult even to speak of simple magnetic Raman scattering. A study of the resonant Raman scattering will be presented elsewhere.

Corrections to LSWT appearing in the form of multiple-magnon excitations are present also in the spin-

spin correlation function or structure factor  $S(\mathbf{k}, \omega)$  at  $T = 0$ , which is the dynamical quantity measured in neutron-scattering experiments. In contrast to the problem of the Raman scattering, the coupling between spins and neutrons is well understood.<sup>15</sup> Therefore both theoretical and experimental studies of the dynamical structure factor are an ideal test of how important are multiple-magnon contributions, which make the model deviate from the LSWT picture. Igarashi and Watabe<sup>6</sup> have computed the spin-wave expansion of the transverse dynamical correlations by the Holstein-Primakoff (HP) transformation and found that the second-order correction gives rise to a sideband with large intensity, corresponding to three-magnon excitations (up to 50% of the dominant one magnon peak for short wavelengths). This result is somewhat at odds with the very small four-magnon continuum obtained in Ref. 13. In a recent work Singh<sup>16</sup> computed the equal-time transverse correlations by series expansion around the Ising limit and used the single-mode approximation to estimate the spin-wave dispersion. He found gapless modes near  $\mathbf{k} = \mathbf{0}$  and  $\mathbf{k} = (\pi, \pi)$  with a spin-wave velocity larger than the one obtained by the renormalized LSWT, signaling indeed the presence of higher magnons in the structure factor. However, the multiple-magnon relative intensity is not as large as in Ref. 6. Neutron-scattering experiments with improved accuracy in undoped and lightly doped cuprates are presently underway. We therefore believe that it is important to have a precise estimate of the multiple-magnon intensity and the frequency dependence of the structure function. This is the central goal of this work.

The first purpose of this paper is to recompute the dynamical transverse correlations by using the Dyson-Maleev (DM) spin-wave formalism. The DM formalism has several advantages over the HP formalism. It is more compact and can handle more easily and safely the singularities of the spin-wave interaction vertices. Furthermore, we will include a careful treatment of the umklapp processes, which are essential to get the second-order correction right.<sup>7</sup> Umklapp processes were not included in Ref. 6, and we believe this is the possible reason for some problems in their results, as we will discuss in this paper. We will show that the three-magnon continuum is not negligible, but still always much smaller than the dominant one-magnon peak. We will compare our integrated intensity and first frequency moment with the equal-time correlations and single-mode approximation obtained by series expansion. As a by-product of the study of the spin-spin correlation function we will evaluate the second-order correction for the transverse spin susceptibility.

In the second part of this paper we shall present a study of the dynamical longitudinal correlation function. One would naively expect that this quantity is not very interesting in the presence of a broken-symmetry situation. However, because of quantum fluctuations, the longitudinal correlation function is nontrivial. We shall see that the longitudinal line shape, to leading order, is the same as the one obtained by the rotationally invariant Schwinger-boson formalism of Arovas and Auerbach in

the mean-field approximation, characterized by two narrow peaks and a one-magnon and a two-magnon excitation. We shall also consider the first-order correction and show how the magnon interaction modifies this two-peak line shape. From the longitudinal correlation function we will extract the staggered magnetization, corrected to second order, and compare our result with those recently reported in the literature. Again, we will show the importance in this calculation of a correct treatment of the umklapp processes.

The paper is organized in the following way. In Sec. II we will define the different correlation functions, which are the subject of this paper, and discuss their meaning. We shall then review the basic elements of SWT in the DM formalism. In Sec. III A we study the transverse correlations, both dynamical and static. The longitudinal part is discussed in Sec. IV. Finally, Sec. V contains the conclusions of this work.

## II. FORMALISM

In this section we give the main definitions of the correlation functions that we are going to calculate, and we summarize the essential elements of the Dyson-Maleev spin-wave theory.

### A. Definitions and general considerations

We consider the isotropic antiferromagnetic Heisenberg model on a 2D square lattice, described by the Hamiltonian

$$H = J \sum_{\langle ij \rangle} \mathbf{S}_i \cdot \mathbf{S}_j, \quad (2.1)$$

where  $J > 0$ , and the sum extends over distinct pairs of nearest neighbors.

We define the time-dependent spin-correlation function

$$S(\mathbf{k}, t) = \langle \mathbf{S}(\mathbf{k}, t) \cdot \mathbf{S}(-\mathbf{k}, 0) \rangle, \quad (2.2)$$

where the angular brackets denote the expectation value in the ground state, and  $S^a(\mathbf{k})$ ,  $a = x, y, z$ , is the Fourier transform of the spin operators, defined as

$$S^a(\mathbf{k}) = \frac{1}{\sqrt{2N}} \sum_i e^{i\mathbf{k} \cdot \mathbf{r}_i} S_i^a. \quad (2.3)$$

We assume that the lattice contains  $2N$  sites. Here  $\mathbf{k}$  is one of the  $2N$  wave vectors in the Brillouin zone of the square lattice (which will be denoted as LBZ). The time-dependent operators in Eq. (2.2) are meant to be in the Heisenberg picture.

The quantity measured in neutron-scattering experiments is the dynamical structure factor, which is given by the time Fourier transform (FT) of the spin-correlation function,

$$S(\mathbf{k}, \omega) = \int_{-\infty}^{+\infty} \frac{dt}{2\pi} e^{i\omega t} S(\mathbf{k}, t). \quad (2.4)$$

By definition  $S(\mathbf{k}, \omega)$  is a real, positive-definite quantity. Furthermore, since we are at zero temperature,  $S(\mathbf{k}, \omega)$  is nonzero only for positive frequencies  $\omega > 0$ .

To study a situation in which the system has a symmetry-broken ground state in the  $z$  direction, it is convenient to write the spin-correlation function as the sum of a transverse component and a longitudinal component,

$$S(\mathbf{k}, t) = P(\mathbf{k}, t) + L(\mathbf{k}, t), \quad (2.5)$$

with the transverse part defined as

$$P(\mathbf{k}, t) = \frac{1}{2}[P^{+-}(\mathbf{k}, t) + P^{-+}(\mathbf{k}, t)], \quad (2.6)$$

where

$$P^{+-}(\mathbf{k}, t) = \langle S^+(\mathbf{k}, t)S^-(-\mathbf{k}, 0) \rangle, \quad (2.7a)$$

$$P^{-+}(\mathbf{k}, t) = \langle S^-(\mathbf{k}, t)S^+(-\mathbf{k}, 0) \rangle, \quad (2.7b)$$

and the longitudinal part

$$L(\mathbf{k}, t) = \langle S^z(\mathbf{k}, t)S^z(-\mathbf{k}, 0) \rangle. \quad (2.8)$$

Here, as usual,

$$S^+(\mathbf{k}) = S^x(\mathbf{k}) + iS^y(\mathbf{k}), \quad (2.9)$$

$$S^-(\mathbf{k}) = S^x(\mathbf{k}) - iS^y(\mathbf{k}). \quad (2.10)$$

The structure factor can be rewritten as

$$S(\mathbf{k}, \omega) = P^{+-}(\mathbf{k}, \omega) + L(\mathbf{k}, \omega). \quad (2.11)$$

In order to obtain Eq. (2.11), the equality  $P^{+-}(\mathbf{k}, \omega) = P^{-+}(\mathbf{k}, \omega)$  has been used.

If the ground state of the system were the naive Néel state, the longitudinal correlation function would have a trivial structure: just an elastic peak at the antiferromagnetic wave vector  $\mathbf{k} = (\pi, \pi)$ . However, even in the presence of a staggered magnetization in the  $z$  direction, quantum fluctuations make the longitudinal part nontrivial.

We shall also consider the "equal-time" correlation function, defined as

$$\begin{aligned} S(\mathbf{k}) &\equiv \langle \mathbf{S}(\mathbf{k}) \cdot \mathbf{S}(-\mathbf{k}) \rangle \\ &= \int_{-\infty}^{+\infty} d\omega S(\mathbf{k}, \omega), \end{aligned} \quad (2.12)$$

which is a useful quantity, in order to characterize the ground state of the Heisenberg model. It can also be measured directly in neutron-scattering experiments by integrating the dynamical structure factor up to high enough frequencies.

## B. Spin-wave theory

We want to evaluate  $P(\mathbf{k}, \omega)$  and  $L(\mathbf{k}, \omega)$  within spin-wave theory, where the existence of a nonzero staggered magnetization in the  $z$  direction is assumed *a priori*.

As in two previous papers<sup>13,7</sup> we use the Dyson-Maleev (DM) transformation<sup>17,18</sup> to represent the spin variables as bosons and therefore map the spin Hamiltonian into a boson Hamiltonian. Details of the DM transformation and the derivation of the DM boson Hamiltonian can be found in Refs. 13 and 7. Here we summarize the main points. The DM Hamiltonian, obtained from the spin Hamiltonian of Eq. (2.1), is the sum of a quadratic term and a quartic term. The quadratic term is diagonalized by a Bogoliubov transformation. The quartic term is expressed in terms of the quasiparticle operators and normal ordered. The total Hamiltonian finally reads

$$H_{DM} = \text{const} + H_0 + V_{DM}. \quad (2.13)$$

The quadratic part  $H_0$  is given by

$$H_0 = \sum_{\mathbf{k}} \Omega_{\max} \epsilon_{\mathbf{k}} (\alpha_{\mathbf{k}}^\dagger \alpha_{\mathbf{k}} + \beta_{\mathbf{k}}^\dagger \beta_{\mathbf{k}}), \quad (2.14)$$

where  $\Omega_{\max} = JzS\alpha(S)$ ,  $\alpha(S) = 1 + 0.157948/2S$ , and  $\epsilon_{\mathbf{k}} = (1 - \gamma_{\mathbf{k}}^2)^{1/2}$ . Here

$$\gamma_{\mathbf{k}} = \frac{1}{z} \sum_{\delta} e^{i\mathbf{a}\mathbf{k}\cdot\delta} = \frac{\cos k_x a + \cos k_y a}{2}, \quad (2.15)$$

and the sum over  $\delta$  is over the  $z = 4$  (for the square lattice) unit vectors connecting site  $i$  with its nearest neighbors.  $a$  is the lattice constant.  $\alpha_{\mathbf{k}}^\dagger$ ,  $\alpha_{\mathbf{k}}$ ,  $\beta_{\mathbf{k}}^\dagger$ , and  $\beta_{\mathbf{k}}$  are magnon creation and annihilation operators.

The quartic part of the Hamiltonian is written as

$$\begin{aligned} V_{DM} = -\frac{zJ}{4N} \sum_{1234} \delta_{\mathbf{G}}(1+2-3-4) & \left[ V_{1234}^{(1)} \alpha_1^\dagger \alpha_2^\dagger \alpha_3 \alpha_4 + V_{1234}^{(2)} \alpha_1^\dagger \beta_2 \alpha_3 \alpha_4 + V_{1234}^{(3)} \alpha_1^\dagger \alpha_2^\dagger \beta_3^\dagger \alpha_4 \right. \\ & + V_{1234}^{(4)} \alpha_1^\dagger \alpha_3 \beta_4^\dagger \beta_2 + V_{1234}^{(5)} \beta_4^\dagger \alpha_3 \beta_2 \beta_1 + V_{1234}^{(6)} \beta_4^\dagger \beta_3^\dagger \alpha_2^\dagger \beta_1 \\ & \left. + V_{1234}^{(7)} \alpha_1^\dagger \alpha_2^\dagger \beta_3^\dagger \beta_4^\dagger + V_{1234}^{(8)} \beta_1 \beta_2 \alpha_3 \alpha_4 + V_{1234}^{(9)} \beta_4^\dagger \beta_3^\dagger \beta_2 \beta_1 \right]. \end{aligned} \quad (2.16)$$

We shall use the abbreviations 1 for  $\mathbf{k}_1$ , 2 for  $\mathbf{k}_2$ , and so on. In Eq. (2.16) the Kronecker delta  $\delta_{\mathbf{G}}(1+2-3-4)$  expresses the conservation of momentum to within a reciprocal-lattice vector  $\mathbf{G}$ . The vertex functions  $V^{(i)} \equiv V_{1234}^{(i)}$ ,  $i = 1, \dots, 9$ , are the DM vertices. Their explicit expressions can be found in Ref. 13, where we discuss how to implement umklapp processes that are possible when  $\mathbf{G} \neq 0$ . The umklapp plays an important role in calculations beyond linear spin-wave theory,<sup>7,14,19</sup> as we shall also see here. The DM transformation is the most convenient and compact way of handling the infrared singularities of the spin-wave interaction vertices.<sup>20</sup>

In terms of the quasiparticle operators  $\alpha$  and  $\beta$ , the Fourier transforms of the single spin variables are, for sublattice  $A$ ,

$$S_A^+(\mathbf{k}) = \frac{1}{\sqrt{N}} \sum_{\mathbf{r}_i \in A} e^{i\mathbf{k} \cdot \mathbf{r}_i} S_i^+ \\ = \sqrt{2S} \left[ Du_{\mathbf{k}}(\alpha_{\mathbf{k}} - x_{\mathbf{k}}\beta_{\mathbf{k}}^\dagger) - \frac{1}{2S} \frac{1}{N} \sum_{234} \delta_{\mathbf{G}}(\mathbf{k} - 2 - 3 - 4) u_2 u_3 u_4 (x_3 x_4 \alpha_2^\dagger \beta_3^\dagger \beta_4^\dagger - x_2 \beta_2 \alpha_3 \alpha_4) \right], \quad (2.17)$$

$$S_A^-(\mathbf{k}) = \frac{1}{\sqrt{N}} \sum_{\mathbf{r}_i \in A} e^{i\mathbf{k} \cdot \mathbf{r}_i} S_i^- = \sqrt{2S} u_{\mathbf{k}} (\alpha_{\mathbf{k}}^\dagger - x_{\mathbf{k}} \beta_{\mathbf{k}}), \quad (2.18)$$

$$S_A^z(\mathbf{k}) = \frac{1}{\sqrt{N}} \sum_{\mathbf{r}_i \in A} e^{i\mathbf{k} \cdot \mathbf{r}_i} S_i^z \\ = \sqrt{N} S D \delta_{\mathbf{k},0} - \frac{1}{\sqrt{N}} \sum_{\mathbf{q}\mathbf{q}'} \delta_{\mathbf{G}}(\mathbf{q} - \mathbf{q}' - \mathbf{k}) u_{\mathbf{q}} u_{\mathbf{q}'} \left[ \alpha_{\mathbf{q}}^\dagger \alpha_{\mathbf{q}'} + x_{\mathbf{q}} x_{\mathbf{q}'} \beta_{\mathbf{q}'}^\dagger \beta_{\mathbf{q}} - x_{\mathbf{q}'} \beta_{\mathbf{q}'}^\dagger \alpha_{\mathbf{q}}^\dagger - x_{\mathbf{q}} \beta_{\mathbf{q}} \alpha_{\mathbf{q}'} \right], \quad (2.19)$$

and for sublattice  $B$ ,

$$S_B^+(\mathbf{k}) = \frac{1}{\sqrt{N}} \sum_{\mathbf{r}_j \in B} e^{i\mathbf{k} \cdot \mathbf{r}_j} S_j^+ \\ = \sqrt{2S} \left[ Du_{\mathbf{k}}(\beta_{\mathbf{k}}^\dagger - x_{\mathbf{k}} \alpha_{\mathbf{k}}) - \frac{1}{2S} \frac{1}{N} \sum_{234} \delta_{\mathbf{G}}(\mathbf{k} - 2 - 3 - 4) \phi_{\mathbf{G}} u_2 u_3 u_4 (x_3 x_4 \beta_2 \alpha_3 \alpha_4 - x_2 \alpha_2^\dagger \beta_3^\dagger \beta_4^\dagger) \right], \quad (2.20)$$

$$S_B^-(\mathbf{k}) = \frac{1}{\sqrt{N}} \sum_{\mathbf{r}_j \in B} e^{i\mathbf{k} \cdot \mathbf{r}_j} S_j^- = \sqrt{2S} u_{\mathbf{k}} (\beta_{\mathbf{k}} - x_{\mathbf{k}} \alpha_{\mathbf{k}}^\dagger), \quad (2.21)$$

$$S_B^z(\mathbf{k}) = \frac{1}{\sqrt{N}} \sum_{\mathbf{r}_j \in B} e^{i\mathbf{k} \cdot \mathbf{r}_j} S_j^z \\ = -\sqrt{N} S D \delta_{\mathbf{k},0} + \frac{1}{\sqrt{N}} \sum_{\mathbf{q}\mathbf{q}'} \delta_{\mathbf{G}}(\mathbf{q} - \mathbf{q}' - \mathbf{k}) \phi_{\mathbf{G}} u_{\mathbf{q}} u_{\mathbf{q}'} \left[ x_{\mathbf{q}} x_{\mathbf{q}'} \alpha_{\mathbf{q}}^\dagger \alpha_{\mathbf{q}'} + \beta_{\mathbf{q}'}^\dagger \beta_{\mathbf{q}} - x_{\mathbf{q}} \beta_{\mathbf{q}'}^\dagger \alpha_{\mathbf{q}}^\dagger - x_{\mathbf{q}'} \beta_{\mathbf{q}} \alpha_{\mathbf{q}'} \right], \quad (2.22)$$

with

$$u_{\mathbf{k}} = \sqrt{\frac{1 + \epsilon_{\mathbf{k}}}{2\epsilon_{\mathbf{k}}}}, \quad (2.23)$$

$$x_{\mathbf{k}} = \sqrt{\frac{1 - \epsilon_{\mathbf{k}}}{1 + \epsilon_{\mathbf{k}}}}. \quad (2.24)$$

$$D = \left( 1 - \frac{1}{SN} \sum_{\mathbf{k}} x_{\mathbf{k}}^2 u_{\mathbf{k}}^2 \right) \\ = \left( 1 - \frac{0.39320}{2S} \right). \quad (2.25)$$

Note that the wave vector  $\mathbf{k}$  of these Fourier transforms lies within the antiferromagnetic Brillouin zone (AFMBZ).  $\mathbf{G}$  is again a reciprocal-lattice vector with respect to the same zone. In Eqs. (2.20) and (2.22), the quantity

$$\phi_{\mathbf{G}} = e^{i\mathbf{a}\mathbf{G} \cdot \delta_x} = e^{i\mathbf{a}\mathbf{G}_x} \quad (2.26)$$

is a phase factor related to the umklapp processes. It arises by taking the FT of the spin variables of the  $B$  sublattice because we have chosen the convention of putting the origin of the coordinates on one site of the  $A$  sublattice, so that  $\mathbf{r}_j = \mathbf{r}_i + \delta_x$ , for  $\mathbf{r}_j \in B$ , where  $\delta_x$  is a unit vector taken (arbitrarily) in the  $x$  direction. The phase  $\phi_{\mathbf{G}}$  can only take the values  $\pm 1$ .

We finally need to relate the Fourier transform defined in Eq. (2.3), where no sublattice decomposition was assumed, to Eqs. (2.17)–(2.22), where we have distin-

guished between sublattices. In order to probe the whole LBZ, which is relevant for experiment, it is not enough to consider

$$S^a(\mathbf{k}) = S_A^a(\mathbf{k}) + S_B^a(\mathbf{k}), \quad (2.27)$$

when  $\mathbf{k}$  is confined inside the AFMBZ. In addition to these variables, which we will call *uniform*, it is necessary to introduce the *staggered* variables

$$Q^a(\mathbf{k}) = S_A^a(\mathbf{k}) - S_B^a(\mathbf{k}). \quad (2.28)$$

Alternatively,  $Q^a(\mathbf{k})$  can be obtained from  $S^a(\mathbf{k})$  if we allow  $\mathbf{k}$  to vary within the LBZ, by unklapping the region {LBZ – AFMBZ} back to AFMBZ through the reciprocal-lattice vector (of the AFMBZ)  $\mathbf{G} = (\pi, \pi)/a$ . This implies that, on the AFMBZ border, staggered and uniform variables are equivalent. Therefore, if we use the sublattice decomposition and take the wave vectors to be inside the AFMBZ, we must introduce and evaluate the following four correlation functions: two transverse correlation functions (uniform and staggered)

$$P_S^{+-}(\mathbf{k}, t) = \langle S^+(\mathbf{k}, t) S^-(\mathbf{k}, 0) \rangle, \quad (2.29)$$

$$P_Q^{+-}(\mathbf{k}, t) = \langle Q^+(\mathbf{k}, t) Q^-(\mathbf{k}, 0) \rangle, \quad (2.30)$$

and two longitudinal (uniform and staggered)

$$L_S(\mathbf{k}, t) = \langle S^z(\mathbf{k}, t) S^z(\mathbf{k}, 0) \rangle, \quad (2.31)$$

$$L_Q(\mathbf{k}, t) = \langle Q^z(\mathbf{k}, t) Q^z(\mathbf{k}, 0) \rangle. \quad (2.32)$$

The staggered correlation functions for  $\mathbf{k}$  close to the zone center actually probe a region around the antiferromagnetic wave vector,  $(\pi, \pi)/a$ .

For the standard many-body treatment of this problem, we finally introduce four corresponding time-ordered Green's functions, with the imaginary part proportional to the spectral densities of the correlation functions defined above. We define

$$\mathcal{P}_S^{+-}(\mathbf{k}, t) = -i\langle TS^+(\mathbf{k}, t)S^-(-\mathbf{k}, 0) \rangle, \quad (2.33)$$

$$\mathcal{P}_Q^{+-}(\mathbf{k}, t) = -i\langle TQ^+(\mathbf{k}, t)Q^-(-\mathbf{k}, 0) \rangle, \quad (2.34)$$

$$\mathcal{L}_S(\mathbf{k}, t) = -i\langle TS^z(\mathbf{k}, t)S^z(-\mathbf{k}, 0) \rangle, \quad (2.35)$$

$$\mathcal{L}_Q(\mathbf{k}, t) = -i\langle TQ^z(\mathbf{k}, t)Q^z(-\mathbf{k}, 0) \rangle. \quad (2.36)$$

We have

$$P_S^{+-}(\mathbf{k}, \omega) = -\frac{1}{\pi}\text{Im} \mathcal{P}_S^{+-}(\mathbf{k}, \omega), \quad (2.37)$$

for  $\omega > 0$ , and so on.

### III. TRANSVERSE SPIN-CORRELATION FUNCTION

In this section we study the transverse spin-correlation function, both dynamical and "equal time," and we compare our results with other works.

#### A. Dynamical structure factor

To make the evaluation of  $\mathcal{P}_S^{+-}(\mathbf{k}, \omega)$  and  $\mathcal{P}_Q^{+-}(\mathbf{k}, \omega)$  in perturbation theory efficient we follow Ref. 21 and introduce a Green's-function matrix in terms of the spin operators

$$2SF_{mn}^{+-}(\mathbf{k}, t) \equiv -i\langle TS_m^+(\mathbf{k}, t)S_n^-(\mathbf{k}, 0) \rangle, \quad (3.1)$$

where  $m, n = A, B$ , and another matrix related to the  $\alpha$  and  $\beta$  quasiparticle operators

$$2SF_{\mu\nu}^{+-}(\mathbf{k}, \omega) \equiv \sum_{m,n} (U_{\mathbf{k}})_{\mu m} F_{mn}^{+-}(\mathbf{k}, \omega) (U_{\mathbf{k}})_{\nu n}, \quad (3.2)$$

where  $m, n = A, B$ , and  $\mu, \nu = \alpha, \beta$ .  $U_{\mathbf{k}}$  is the matrix of the Bogoliubov transformation defining the  $\alpha$  and  $\beta$  operators:

$$(U_{\mathbf{k}})_{\alpha A} = (U_{\mathbf{k}})_{\beta B} = u_{\mathbf{k}}, \quad (3.3)$$

$$(U_{\mathbf{k}})_{\alpha B} = (U_{\mathbf{k}})_{\beta A} = u_{\mathbf{k}}x_{\mathbf{k}}. \quad (3.4)$$

The Green's functions  $\mathcal{P}_S^{+-}(\mathbf{k}, \omega)$  and  $\mathcal{P}_Q^{+-}(\mathbf{k}, \omega)$  can now be written in a compact way in terms of  $F_{\mu\nu}^{+-}(\mathbf{k}, \omega)$ :

$$\mathcal{P}_S^{+-}(\mathbf{k}, \omega) = 2S[u_{\mathbf{k}}(1-x_{\mathbf{k}})]^2 [F_{\alpha\alpha}^{+-}(\mathbf{k}, \omega) + F_{\beta\beta}^{+-}(\mathbf{k}, \omega) + F_{\alpha\beta}^{+-}(\mathbf{k}, \omega) + F_{\beta\alpha}^{+-}(\mathbf{k}, \omega)], \quad (3.5)$$

$$\mathcal{P}_Q^{+-}(\mathbf{k}, \omega) = 2S[u_{\mathbf{k}}(1+x_{\mathbf{k}})]^2 [F_{\alpha\alpha}^{+-}(\mathbf{k}, \omega) + F_{\beta\beta}^{+-}(\mathbf{k}, \omega) - F_{\alpha\beta}^{+-}(\mathbf{k}, \omega) - F_{\beta\alpha}^{+-}(\mathbf{k}, \omega)]. \quad (3.6)$$

Using Eqs. (2.17)–(2.22) together with Eq. (3.2) one can finally write  $F_{\mu\nu}^{+-}(\mathbf{k}, t)$  in terms of the Green's functions of  $\alpha$  and  $\beta$ :

$$F_{\alpha\alpha}^{+-}(\mathbf{k}, t) = DG_{\alpha\alpha}(\mathbf{k}, t) + \frac{i}{2SN} \sum_{234} \delta_{\mathbf{G}}(\mathbf{k} + 2 - 3 - 4) u_{\mathbf{k}} u_2 u_3 u_4 \times \left[ M_{\mathbf{k}234}^{(1)} \langle T\beta_2(t)\alpha_3(t)\alpha_4(t)\alpha_{\mathbf{k}}^{\dagger}(0) \rangle + M_{\mathbf{k}234}^{(2)} \langle T\alpha_2^{\dagger}(t)\beta_3^{\dagger}(t)\beta_4^{\dagger}(t)\alpha_{\mathbf{k}}^{\dagger}(0) \rangle \right], \quad (3.7a)$$

$$F_{\beta\beta}^{+-}(\mathbf{k}, t) = DG_{\beta\beta}(\mathbf{k}, t) + \frac{i}{2SN} \sum_{234} \delta_{\mathbf{G}}(\mathbf{k} + 2 - 3 - 4) \phi_{\mathbf{G}} u_{\mathbf{k}} u_2 u_3 u_4 \times \left[ M_{\mathbf{k}234}^{(1)} \langle T\alpha_2^{\dagger}(t)\beta_3^{\dagger}(t)\beta_4^{\dagger}(t)\beta_{\mathbf{k}}(0) \rangle + M_{\mathbf{k}234}^{(2)} \langle T\beta_2(t)\alpha_3(t)\alpha_4(t)\beta_{\mathbf{k}}(0) \rangle \right], \quad (3.7b)$$

$$F_{\alpha\beta}^{+-}(\mathbf{k}, t) = DG_{\alpha\beta}(\mathbf{k}, t) + \frac{i}{2SN} \sum_{234} \delta_{\mathbf{G}}(\mathbf{k} + 2 - 3 - 4) u_{\mathbf{k}} u_2 u_3 u_4 \times \left[ M_{\mathbf{k}234}^{(1)} \langle T\beta_2(t)\alpha_3(t)\alpha_4(t)\beta_{\mathbf{k}}(0) \rangle + M_{\mathbf{k}234}^{(2)} \langle T\alpha_2^{\dagger}(t)\beta_3^{\dagger}(t)\beta_4^{\dagger}(t)\beta_{\mathbf{k}}(0) \rangle \right], \quad (3.7c)$$

$$F_{\beta\alpha}^{+-}(\mathbf{k}, t) = DG_{\beta\alpha}(\mathbf{k}, t) + \frac{i}{2SN} \sum_{234} \delta_{\mathbf{G}}(\mathbf{k} + 2 - 3 - 4) \phi_{\mathbf{G}} u_{\mathbf{k}} u_2 u_3 u_4 \times \left[ M_{\mathbf{k}234}^{(1)} \langle T\alpha_2^{\dagger}(t)\beta_3^{\dagger}(t)\beta_4^{\dagger}(t)\alpha_{\mathbf{k}}^{\dagger}(0) \rangle + M_{\mathbf{k}234}^{(2)} \langle T\beta_2(t)\alpha_3(t)\alpha_4(t)\alpha_{\mathbf{k}}^{\dagger}(0) \rangle \right], \quad (3.7d)$$

with

$$M_{\mathbf{k}234}^{(1)} = -x_2 + \phi_{\mathbf{G}} x_{\mathbf{k}} x_3 x_4, \quad (3.8a)$$

$$M_{\mathbf{k}234}^{(2)} = x_3 x_4 - \phi_{\mathbf{G}} x_{\mathbf{k}} x_2. \quad (3.8b)$$

The four components of the matrix  $G_{\mu\nu}(\mathbf{k}, t)$  are the one-particle Green's functions for the  $\alpha$  and  $\beta$  operators:

$$iG_{\alpha\alpha}(\mathbf{k}, t) = \langle T\alpha_{\mathbf{k}}(t)\alpha_{\mathbf{k}}^{\dagger}(0) \rangle, \quad (3.8c)$$

$$iG_{\beta\beta}(\mathbf{k}, t) = \langle T\beta_{\mathbf{k}}^{\dagger}(t)\beta_{\mathbf{k}}(0) \rangle, \quad (3.8d)$$

$$iG_{\alpha\beta}(\mathbf{k}, t) = \langle T\alpha_{\mathbf{k}}(t)\beta_{\mathbf{k}}(0) \rangle, \quad (3.8e)$$

$$iG_{\beta\alpha}(\mathbf{k}, t) = \langle T\beta_{\mathbf{k}}^{\dagger}(t)\alpha_{\mathbf{k}}^{\dagger}(0) \rangle. \quad (3.8f)$$

The Green's functions  $G_{\mu\nu}$  satisfy a matrix Dyson's equation<sup>21</sup>

$$G_{\mu\nu}(\mathbf{k}, \omega) = G_{\mu\nu}^{(0)}(\mathbf{k}, \omega) + \sum_{\gamma\delta} G_{\mu\gamma}^{(0)}(\mathbf{k}, \omega) \Sigma_{\gamma\delta}(\mathbf{k}, \omega) G_{\delta\nu}(\mathbf{k}, \omega), \quad (3.9)$$

where  $G_{\mu\nu}^{(0)}(\mathbf{k}, \omega)$  are the bare propagators

$$G_{\alpha\alpha}^{(0)}(\mathbf{k}, \omega) = \frac{1}{\Omega_{\max}} \frac{1}{\tilde{\omega} - \epsilon_{\mathbf{k}} + i\eta}, \quad (3.10)$$

$$G_{\beta\beta}^{(0)}(\mathbf{k}, \omega) = -\frac{1}{\Omega_{\max}} \frac{1}{\tilde{\omega} + \epsilon_{\mathbf{k}} - i\eta}, \quad (3.11)$$

$$G_{\alpha\beta}^{(0)}(\mathbf{k}, \omega) = G_{\beta\alpha}^{(0)}(\mathbf{k}, \omega) = 0, \quad (3.12)$$

with  $\tilde{\omega} = \omega/\Omega_{\max}$ . The self-energy  $\Sigma_{\gamma\delta}(\mathbf{k}, \omega)$  can be expressed in the usual kind of diagrammatics. The unperturbed  $\alpha$  propagator  $G_{\alpha\alpha}^{(0)}(\mathbf{k}, \omega)$  will be represented by a single-arrow line, and the unperturbed  $\beta$  propagator  $G_{\beta\beta}^{(0)}(\mathbf{k}, \omega)$  will be represented by a double-arrow line. (We will follow the diagrammatical rules and conventions used in Ref. 13.)

The first-order correction to the self-energy, which is of order  $\mathcal{O}(1/S)$  [here we disregard an overall factor  $\Omega_{\max} = JzS\alpha(S)$ ], is identically zero at  $T = 0$ . The second-order self-energy,<sup>22</sup> which is of order  $\mathcal{O}(1/S^2)$ , has been studied in detail in Refs. 13, 7, and 14. There it was shown that the second-order self-energy *on shell* is small and positive, making the magnon dispersion 2–4% stiffer. The correct treatment of the umklapp is essential to obtain these results.

We now need to carry out a similar perturbation expansion for the four Green's functions appearing inside the square brackets of Eqs. (3.7a)–(3.7d):

$$\langle T\beta_2(t)\alpha_3(t)\alpha_4(t)\alpha_{\mathbf{k}}^{\dagger}(0) \rangle, \quad (3.13a)$$

$$\langle T\beta_2(t)\alpha_3(t)\alpha_4(t)\beta_{\mathbf{k}}(0) \rangle, \quad (3.13b)$$

$$\langle T\alpha_2^{\dagger}(t)\beta_3^{\dagger}(t)\beta_4^{\dagger}(t)\alpha_{\mathbf{k}}^{\dagger}(0) \rangle, \quad (3.13c)$$

$$\langle T\alpha_2^{\dagger}(t)\beta_3^{\dagger}(t)\beta_4^{\dagger}(t)\beta_{\mathbf{k}}(0) \rangle. \quad (3.13d)$$

Note that these Green's functions appear multiplied by a factor of  $1/2S$ . Therefore, since we know that each interaction carries essentially a factor of  $1/2S$ , a naive  $1/S$  power counting suggests that it is enough to expand these

Green's function up to first order in perturbation theory, to have a consistent series in  $1/2S$  to second order. The zeroth-order contribution is identically zero. To first order there is just one Feynman diagram contributing to each of these four Green's functions. They are shown in Fig. 1 and are easily evaluated by standard many-body techniques. We can now write the matrix  $F_{\mu\nu}^{+-}(\mathbf{k}, \omega)$ , expanded to this order, in the following compact form:

$$F_{\mu\nu}^{+-}(\mathbf{k}, \omega) = \frac{1}{\Omega_{\max}} [D\tilde{G}_{\mu\nu}(\mathbf{k}, \omega) + I_{\mu\nu}(\mathbf{k}, \omega)\tilde{G}_{\nu\nu}^{(0)}(\mathbf{k}, \omega)], \quad (3.14)$$

with  $\tilde{G}_{\mu\nu} = \Omega_{\max} G_{\mu\nu}$ . The explicit expressions of the functions  $I_{\mu\nu}(\mathbf{k}, \omega)$  are given in the Appendix, where we also report the formulas for the second-order self-energy  $\Sigma_{\mu\nu}^{(2)}(\mathbf{k}, \omega)$ . There is another more fundamental reason to stop after first order in the evaluation of Green's functions given in Eqs. (3.13). This is due to the fact that the expansion parameter of SWT is not simply  $1/S$ , but a more subtle quantity related to the average boson occupation number,<sup>2,8</sup> which is roughly proportional to  $1/z$ .<sup>23,21</sup> This is the reason that SWT is an expansion in  $1/zS$  rather than  $1/S$ . The  $1/z$  power of a given diagram is in turn related to the number of independent momentum labels which is eventually summed over.<sup>24</sup> As shown in the Appendix, the first-order correction involves phase-space integrals of the same order as the second-order correction to the self-energy. Therefore it will have the same  $1/z$  power.

The formulas for  $F_{\mu\nu}^{+-}(\mathbf{k}, \omega)$  obtained here are considerably simpler than the corresponding ones derived by Igarashi and Watabe<sup>6</sup> using the Holstein-Primakoff formalism. We are interested in the imaginary part of  $F_{\mu\nu}^{+-}(\mathbf{k}, \omega)$ . Let us consider the two terms in  $F_{\mu\nu}^{+-}(\mathbf{k}, \omega)$  separately. For  $G_{\mu\nu}(\mathbf{k}, \omega)$ , we need expressions in terms of the self-energy derived through Dyson's equations<sup>21</sup>

$$\tilde{G}_{\alpha\alpha}(\mathbf{k}, \tilde{\omega}) = \frac{1}{\tilde{\omega} - \epsilon_{\mathbf{k}} - \tilde{\Sigma}_{\alpha\alpha}(\mathbf{k}, \tilde{\omega}) + i\eta}, \quad (3.15a)$$

$$\tilde{G}_{\beta\beta}(\mathbf{k}, \tilde{\omega}) = \frac{-1}{\tilde{\omega} + \epsilon_{\mathbf{k}} + \tilde{\Sigma}_{\beta\beta}(\mathbf{k}, \tilde{\omega}) - i\eta}, \quad (3.15b)$$

$$\tilde{G}_{\alpha\beta}(\mathbf{k}, \tilde{\omega}) = \tilde{\Sigma}_{\alpha\beta}(\mathbf{k}, \tilde{\omega})\tilde{G}_{\alpha\alpha}(\mathbf{k}, \tilde{\omega})\tilde{G}_{\beta\beta}(\mathbf{k}, \tilde{\omega}), \quad (3.15c)$$

$$\tilde{G}_{\beta\alpha}(\mathbf{k}, \tilde{\omega}) = \tilde{\Sigma}_{\beta\alpha}(\mathbf{k}, \tilde{\omega})\tilde{G}_{\alpha\alpha}(\mathbf{k}, \tilde{\omega})\tilde{G}_{\beta\beta}(\mathbf{k}, \tilde{\omega}), \quad (3.15d)$$

with  $\tilde{\Sigma}_{\mu\nu}(\mathbf{k}, \tilde{\omega}) = \frac{1}{\Omega_{\max}} \Sigma_{\mu\nu}(\mathbf{k}, \tilde{\omega})$ . In evaluating the spec-

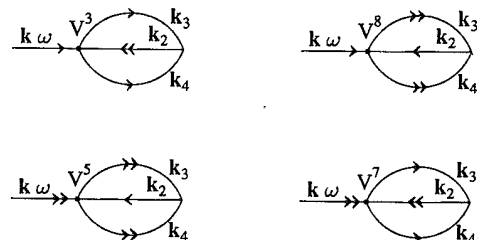


FIG. 1. Four diagrams contributing, respectively, to the four Green's functions given in Eqs. (3.13) to first order.

tral density of  $G_{\mu\nu}$  we need to distinguish between the region (in  $\omega$ ) characterized by a dominant  $\delta$ -function-like peak, corresponding to one-magnon excitations, and the region where a nonzero imaginary part of  $\Sigma_{\mu\nu}$  gives rise to a sideband corresponding to three-magnon excitations. In the first case we are considering  $\tilde{\omega}$  close to its *resonance* value. If we are interested only in positive frequencies  $\tilde{\omega} > 0$ , this resonance happens only in  $G_{\alpha\alpha}$ , when

$$\tilde{\omega} \approx \epsilon_{\mathbf{k}} + \tilde{\Sigma}_{\alpha\alpha}(\mathbf{k}, \epsilon_{\mathbf{k}}). \quad (3.16)$$

In this region the imaginary part of  $\tilde{\Sigma}_{\alpha\alpha}$  is negligible, and we can make the single-pole approximation

$$\begin{aligned} \text{Im } \tilde{G}_{\alpha\alpha}(\mathbf{k}, \tilde{\omega}) &= -\pi\delta(\tilde{\omega} - \epsilon_{\mathbf{k}} - \text{Re } \tilde{\Sigma}_{\alpha\alpha}(\mathbf{k}, \tilde{\omega})) \\ &= -\pi\delta(\tilde{\omega} - \epsilon_{\mathbf{k}})Z(\mathbf{k}), \end{aligned} \quad (3.17)$$

with

$$\begin{aligned} Z(\mathbf{k}) &= \left[1 - \frac{\partial}{\partial \tilde{\omega}} \tilde{\Sigma}_{\alpha\alpha}(\mathbf{k}, \tilde{\omega})\right]_{\tilde{\omega}=\epsilon_{\mathbf{k}}}^{-1} \\ &\approx \left[1 + \frac{\partial}{\partial \tilde{\omega}} \tilde{\Sigma}_{\alpha\alpha}(\mathbf{k}, \tilde{\omega})\right]_{\tilde{\omega}=\epsilon_{\mathbf{k}}}. \end{aligned} \quad (3.18)$$

There is no spin-wave peak in the spectral density of  $\tilde{G}_{\beta\beta}$  for  $\tilde{\omega} > 0$ . For  $\tilde{G}_{\alpha\beta}$  and  $\tilde{G}_{\beta\alpha}$  the  $\delta$ -function peak again comes from  $\tilde{G}_{\alpha\alpha}$  [see Eqs. (3.15c)–(3.15d)],

$$\text{Im } \tilde{G}_{\alpha\beta}(\mathbf{k}, \tilde{\omega}) = -\pi\delta(\tilde{\omega} - \epsilon_{\mathbf{k}}) \left[ -\frac{1}{\tilde{\omega} + \epsilon_{\mathbf{k}}} \tilde{\Sigma}_{\alpha\beta}(\mathbf{k}, \epsilon_{\mathbf{k}}) \right], \quad (3.19)$$

$$\text{Im } \tilde{G}_{\beta\alpha}(\mathbf{k}, \tilde{\omega}) = -\pi\delta(\tilde{\omega} - \epsilon_{\mathbf{k}}) \left[ -\frac{1}{\tilde{\omega} + \epsilon_{\mathbf{k}}} \tilde{\Sigma}_{\beta\alpha}(\mathbf{k}, \epsilon_{\mathbf{k}}) \right]. \quad (3.20)$$

The second contribution to the spectral function of  $G_{\mu\nu}$  comes from regions where  $\tilde{\Sigma}_{\mu\nu}(\mathbf{k}, \tilde{\omega}) \neq 0$  and has a branch cut on the real axis. In this case we get

$$\begin{aligned} \text{Im } \tilde{G}_{\alpha\alpha}(\mathbf{k}, \tilde{\omega}) &= \frac{\text{Im } \tilde{\Sigma}_{\alpha\alpha}(\mathbf{k}, \tilde{\omega})}{[\tilde{\omega} - \epsilon_{\mathbf{k}} - \text{Re } \tilde{G}_{\alpha\alpha}(\mathbf{k}, \tilde{\omega})]^2 + [\text{Im } \tilde{\Sigma}_{\alpha\alpha}(\mathbf{k}, \tilde{\omega})]^2} \\ &\approx \frac{\text{Im } \tilde{\Sigma}_{\alpha\alpha}(\mathbf{k}, \tilde{\omega})}{(\tilde{\omega} - \epsilon_{\mathbf{k}})^2}, \end{aligned} \quad (3.21)$$

where we have neglected the self-energy in the denominator, because  $\text{Im } \tilde{\Sigma}_{\alpha\alpha}$  is already second order in perturbation theory. Similar expressions are obtained for the other components of the self-energy.

The second term in Eq. (3.14),  $I_{\mu\nu}(\mathbf{k}, \omega) \tilde{G}_{\nu\nu}^{(0)}(\mathbf{k}, \omega)$ , can be treated in a very similar way. Now the  $\delta$ -function peak comes trivially from  $\tilde{G}_{\nu\nu}^{(0)}(\mathbf{k}, \omega)$ . Therefore the final expression of the spectral functions of  $F_{\mu\nu}(\mathbf{k}, \omega)$  are (1) the  $\delta$ -function peak

$$\text{Im } F_{\alpha\alpha}^{+-}(\mathbf{k}, \omega) = (-\pi) \frac{D}{\Omega_{\max}} \delta(\tilde{\omega} - \epsilon_{\mathbf{k}}) \left[ 1 + \frac{\partial}{\partial \tilde{\omega}} \tilde{\Sigma}_{\alpha\alpha}(\mathbf{k}, \epsilon_{\mathbf{k}}) + \frac{1}{D} I_{\alpha\alpha}(\mathbf{k}, \epsilon_{\mathbf{k}}) \right], \quad (3.22a)$$

$$\text{Im } F_{\beta\beta}^{+-}(\mathbf{k}, \omega) = 0, \quad (3.22b)$$

$$\text{Im } F_{\alpha\beta}^{+-}(\mathbf{k}, \omega) = (-\pi) \frac{D}{\Omega_{\max}} \delta(\tilde{\omega} - \epsilon_{\mathbf{k}}) \left[ -\frac{1}{\tilde{\omega} + \epsilon_{\mathbf{k}}} \tilde{\Sigma}_{\alpha\beta}(\mathbf{k}, \epsilon_{\mathbf{k}}) \right], \quad (3.22c)$$

$$\text{Im } F_{\beta\alpha}^{+-}(\mathbf{k}, \omega) = (-\pi) \frac{D}{\Omega_{\max}} \delta(\tilde{\omega} - \epsilon_{\mathbf{k}}) \left[ -\frac{1}{\tilde{\omega} + \epsilon_{\mathbf{k}}} \tilde{\Sigma}_{\beta\alpha}(\mathbf{k}, \epsilon_{\mathbf{k}}) + \frac{1}{D} I_{\beta\alpha}(\mathbf{k}, \epsilon_{\mathbf{k}}) \right], \quad (3.22d)$$

and (2) the three-magnon continuum

$$\text{Im } F_{\alpha\alpha}^{+-}(\mathbf{k}, \omega) = \frac{D}{\Omega_{\max}} \left[ \frac{1}{(\tilde{\omega} - \epsilon_{\mathbf{k}})^2} \text{Im } \tilde{\Sigma}_{\alpha\alpha}(\mathbf{k}, \tilde{\omega}) + \frac{1}{D} \frac{1}{\tilde{\omega} - \epsilon_{\mathbf{k}}} \text{Im } I_{\alpha\alpha}(\mathbf{k}, \tilde{\omega}) \right], \quad (3.23a)$$

$$\text{Im } F_{\beta\beta}^{+-}(\mathbf{k}, \omega) = \frac{D}{\Omega_{\max}} \left[ \frac{1}{(\tilde{\omega} + \epsilon_{\mathbf{k}})^2} \text{Im } \tilde{\Sigma}_{\beta\beta}(\mathbf{k}, \tilde{\omega}) - \frac{1}{D} \frac{1}{\tilde{\omega} + \epsilon_{\mathbf{k}}} \text{Im } I_{\beta\beta}(\mathbf{k}, \tilde{\omega}) \right], \quad (3.23b)$$

$$\text{Im } F_{\alpha\beta}^{+-}(\mathbf{k}, \omega) = \frac{D}{\Omega_{\max}} \left[ -\frac{1}{\tilde{\omega}^2 - \epsilon_{\mathbf{k}}^2} \text{Im } \tilde{\Sigma}_{\alpha\beta}(\mathbf{k}, \tilde{\omega}) - \frac{1}{D} \frac{1}{\tilde{\omega} + \epsilon_{\mathbf{k}}} \text{Im } I_{\alpha\beta}(\mathbf{k}, \tilde{\omega}) \right], \quad (3.23c)$$

$$\text{Im } F_{\beta\alpha}^{+-}(\mathbf{k}, \omega) = \frac{D}{\Omega_{\max}} \left[ -\frac{1}{\tilde{\omega}^2 - \epsilon_{\mathbf{k}}^2} \text{Im } \tilde{\Sigma}_{\beta\alpha}(\mathbf{k}, \tilde{\omega}) + \frac{1}{D} \frac{1}{\tilde{\omega} - \epsilon_{\mathbf{k}}} \text{Im } I_{\beta\alpha}(\mathbf{k}, \tilde{\omega}) \right]. \quad (3.23d)$$

These expressions are again considerably simpler than the corresponding ones obtained by Igarashi and Watabe using the HP formalism.<sup>6</sup> Another difference with Ref. 6 is that we have kept all the factors  $D, \alpha$  as they come out from second-order perturbation theory, without explicitly expanding them in  $1/S$ . We have seen that the perturbation theory in the magnon interaction is something more subtle than a naive expansion in  $1/S$ . In particular, the normal ordering of the spin operators introduces quite naturally corrections to infinite order in  $1/S$ , which we prefer to keep unexpanded, having in mind mainly the  $S = 1/2$  case. Finally, our expressions for the functions  $I$ 's contain the umklapp phases, which were completely disregarded in Ref. 6.

We have evaluated Eqs. (3.22) and (3.23a) for several wave vectors in the AFMBZ, by numerical computation of the various phase-space integrals in two different ways, that is, by lattice summation and the Monte Carlo method. The perfect agreement of the results obtained independently from these two techniques gives us confidence in our numerical results. This is especially important in the calculation of the multidimensional integrals defining the  $I$  functions, whose integrands contain infrared singularities. As we discuss below it turns out that the largest second-order contribution to the dynamical transverse structure factor will come from these terms. On the other hand, as previously mentioned, the infrared singularities exactly cancel in the second-order calculation of the self-energy, when the Dyson-Maleev vertices are used, and the self-energy contribution to the spectral function is rather small.

In Figs. 2 and 3 we show plots of the transverse stag-

gered and uniform structure factor for five different wave vectors. As expected, the spectral functions are characterized by a  $\delta$ -function peak, located at the one-magnon excitation energy  $\epsilon_{\mathbf{k}}$ , and a sideband of three-magnon excitations.

The transverse spectral function in LSWT approximation has just a one-magnon peak with weight 1. The first-order correction comes from normal ordering the cubic terms of the spin variables [see Eqs. (2.17) and (2.20)] and simply renormalizes the intensity of the one-magnon peak by a factor of  $D$ . This is easy to understand. The normal ordering, or Oguchi's correction, introduces fluctuations which reduce the magnetization and therefore the spectral weight of creating a single spin wave. The second-order corrections cause both the further renormalization of the one-magnon peak and the appearance of the three-magnon continuum. The latter is the result of the *off-shell* decay of the one-magnon excitations, due to the nonlinearities of the spin variables and the Hamiltonian. Note that this process is possible only for energies larger than the one-magnon energy, which is a threshold for the spectral density. The second-order correction slightly modifies the intensity of the  $\delta$ -function peak. For the uniform part, this correction is always negative and larger at the zone center, where it is  $\approx 5\%$  of the first-order result, whereas it is less than 1% for wave vectors near the zone boundary. For the staggered part, the intensity of the  $\delta$ -function peak increases by 3% at the zone center and decreases by less than 1% at the zone boundary. For both the staggered and uniform correlation functions, the absolute three-magnon intensity is very small at the zone center, where it is only 1.5% of the

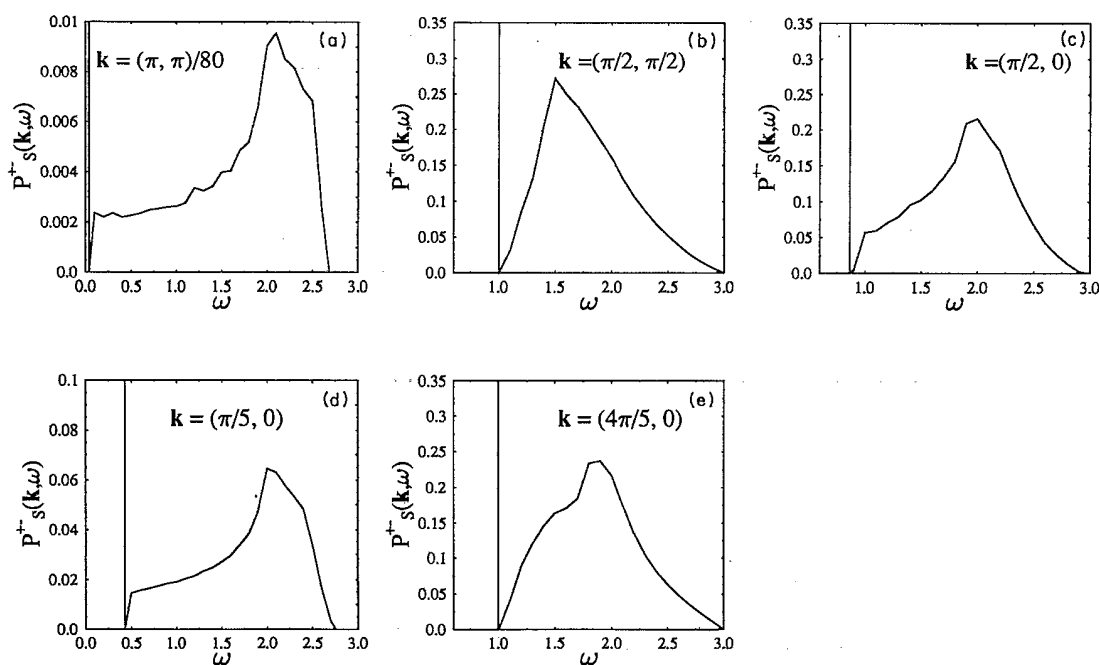


FIG. 2. Dynamical transverse uniform structure factor as a function of the frequency (in units of  $\Omega_{\max}$ ) for several values of the wave vector. (d) and (e) are the cases considered in Ref. 6.

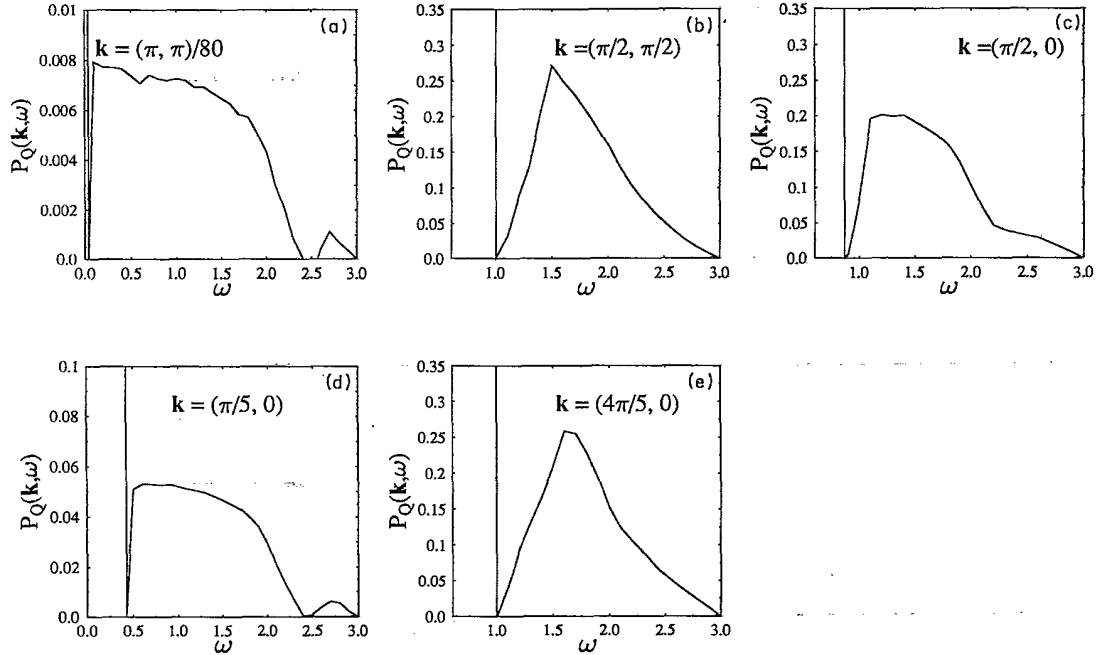


FIG. 3. Dynamical transverse staggered structure factor as a function of the frequency (in units of  $\Omega_{\max}$ ) for several values of the wave vector. (d) and (e) are the cases considered in Ref. 6. For wave vectors on the boundary of the AFMBZ the staggered part is identical to the uniform part.

$\delta$ -function peak, but it becomes increasingly important when the wave vector moves from the zone center to the zone boundary. Here it is approximately 23% of the one-magnon peak. These details are summarized in Table I. Note that the uniform and staggered spectral functions are identical for wave vectors located exactly on the zone boundary, as one would expect from the definition of the staggered part. A correct treatment of the umklapp phases is essential to get this point right. Figs. 2(d), 2(e), 3(d), and 3(e) show the spectral functions for the two wave vectors considered by Igarashi and Watabe.<sup>6</sup> Comparing our results with theirs, we see that the main features of the line shapes are similar, but there are important quantitative differences, especially for wave vectors close to the zone boundary. In con-

trast with our results, their second-order correction of the one-magnon peak is very large and the three-magnon sideband much more intense. For example, their uniform spectral density for  $\mathbf{k} = \frac{129}{160}\pi(1, 0)$  has a sideband intensity which is about 50% of the strongly decreased one-magnon peak. Leaving out the possibility of numerical errors, the reason of the discrepancy must lie either in the different formalism (HP instead of DM) or, more likely, in the fact in Ref. 6 the umklapp processes were neglected. Indeed, for the wave vector  $\mathbf{k} = \frac{129}{160}\pi(1, 0)$ , the uniform and staggered spectral functions of Ref. 6 are rather different, in contrast to what is expected for  $\mathbf{k}$  close to the zone boundary [cf. Figs. 2(e) and 3(e)]. Furthermore, in a more recent work Igarashi<sup>25</sup> recomputed the second-order correction to the spin-wave dispersion,

TABLE I. This table summarizes the results for the integrated intensity of the transverse structure factor, uniform (unif) and staggered (stag), for various wave vectors. The second column contains the absolute intensity of the  $\delta$ -function peak, the third column the absolute intensity of the three-magnon continuum; the fourth column the total integrated intensity, and the sixth column the ratio (in %) of the  $\delta$ -function intensity to the three-magnon continuum.

$\mathbf{k}$	$\delta$ peak	Three-magnon	Total	Three-magnon/ $\delta$ peak (%)
$(1, 1) \frac{\pi}{80}$ (stag)	0.625	0.0085	0.633	1.355
$(1, 1) \frac{\pi}{80}$ (unif)	0.572	0.0067	0.578	1.176
$(1, 1) \frac{\pi}{80}$ (stag)	0.601	0.1389	0.740	23.10
$(1, 1) \frac{\pi}{80}$ (unif)	0.601	0.1389	0.704	23.10
$(1, 0) \frac{\pi}{5}$ (stag)	0.613	0.1296	0.743	21.13
$(1, 0) \frac{\pi}{5}$ (unif)	0.586	0.1240	0.710	21.16
$(1, 0) \frac{\pi}{5}$ (stag)	0.622	0.0702	0.702	12.84
$(1, 0) \frac{\pi}{5}$ (unif)	0.573	0.0693	0.642	12.10
$(1, 0) \frac{4\pi}{5}$ (stag)	0.603	0.1389	0.742	23.02
$(1, 0) \frac{4\pi}{5}$ (unif)	0.602	0.1380	0.740	22.93

including a correct treatment of the umklapp, and obtained the same result as us in Ref. 7. This seems to imply that the HP and DM formalisms give equivalent results when consistently applied. In fact, the equivalence of the two formalisms in the calculation of *on-shell* quantities had been already recognized a long time ago by Harris *et al.*<sup>21</sup> who, however, pointed out that the HP formalism, in contrast to the DM formalism, is not automatically self-consistent in calculations off the mass shell, and so in these cases the two formalisms may disagree. Therefore even if we believe that the main reason of the disagreement with Ref. 6 is the missing umklapp treatment, we cannot completely rule out the possibility that HP and DM give a different result for this particular calculation, where off-shell processes play an important role. Finally, a small but noticeable feature in the staggered spectral function for wave vectors close to the zone center is the tiny secondary sideband peak that is present in our line shape at a frequency around  $\tilde{\omega} = 2.8$  and which is absent in the corresponding line shapes of Ref. 6. Again, we ascribe this peak to umklapp processes which are clearly more important for high frequencies or short wavelengths.

### B. "Equal-time" structure factor and single-mode approximation

In this section we will consider the "equal-time" transverse correlation functions, staggered and uniform,

$$P_S^{+-}(\mathbf{k}) = \langle S^+(\mathbf{k})S^-(-\mathbf{k}) \rangle = \int_{-\infty}^{+\infty} d\omega P_S^{+-}(\mathbf{k}, \omega), \quad (3.24)$$

$$P_Q^{+-}(\mathbf{k}) = \langle Q^+(\mathbf{k})Q^-(-\mathbf{k}) \rangle = \int_{-\infty}^{+\infty} d\omega P_Q^{+-}(\mathbf{k}, \omega). \quad (3.25)$$

Both  $P_S^{+-}(\mathbf{k})$  and  $P_Q^{+-}(\mathbf{k})$  are easily evaluated by integrating over the frequency the corresponding dynamical structure factors studied in the previous section. As we explained in Sec. I, from the knowledge of the uniform and staggered components inside the AFMBZ we can easily reconstruct the total transverse correlation function  $P^{+-}(\mathbf{k})$  inside the LBZ, which is the quantity we are ultimately interested in.

$P^{+-}(\mathbf{k})$  can give us a quantitative estimate of how our approximations for the correlation functions deviate from LSWT. More importantly, we can compare our results for  $P^{+-}(\mathbf{k})$  with the results obtained recently by Singh<sup>16</sup> by a series expansion around the Ising limit, believed to be very accurate.

In the LSWT approximation the equal-time correlation function is

$$P_S^{+-}(\mathbf{k}) = 2Su_k^2(1 - x_k)^2, \quad (3.26a)$$

$$P_Q^{+-}(\mathbf{k}) = 2Su_k^2(1 + x_k)^2. \quad (3.26b)$$

Since  $x_k \approx 1 - k\sqrt{2}$  for  $\mathbf{k} \approx 0$ ,  $P_S^{+-}(\mathbf{k})$  vanishes linearly, whereas  $P_Q^{+-}(\mathbf{k})$  diverges like  $1/k$  at the zone center. These LSWT results give us a hint of how the equal-time

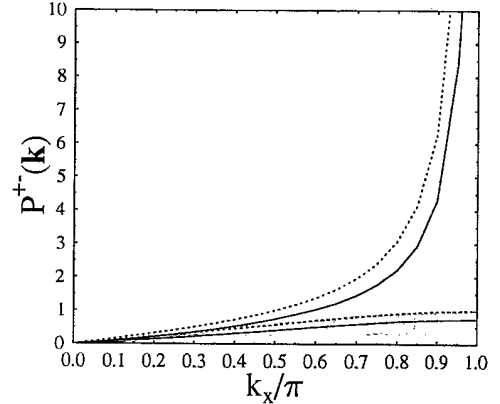


FIG. 4. Plot of  $P^{+-}(\mathbf{k})$  as a function of  $k_x$ , along the directions  $k_x = k_y$  and  $k_y = 0$  in momentum space. The dotted line is the LSWT approximation; the solid line is the second-order SWT. For  $k_x = 0$  to  $k_x = 0.5$ ,  $P^{+-}(\mathbf{k})$  is equivalent to the uniform  $P_S^{+-}(\mathbf{k})$ , whereas for  $k_x = 0.5$  to  $k_x = 1$ ,  $P^{+-}(\mathbf{k})$  coincides with the staggered  $P_Q^{+-}(\mathbf{k})$ .

correlation function  $P^{+-}(\mathbf{k})$  may behave near  $\mathbf{k} = 0$ , and  $\mathbf{k} = (\pi, \pi)$ , respectively, and suggest that to study  $P^{+-}(\mathbf{k})$  in these two limits it is useful<sup>16</sup> also to evaluate  $P_S^{+-}(\mathbf{k})/k$  and  $kP_Q^{+-}(\mathbf{k})$  near  $\mathbf{k} = 0$ . In Fig. 4 we show  $P^{+-}(\mathbf{k})$  along different directions in momentum space of the LBZ. In Figs. 5 and 6 we have instead plotted  $P_S^{+-}(\mathbf{k})/k$  and  $kP_Q^{+-}(\mathbf{k})$ , respectively, along different directions in momentum space of the AFMBZ. The dotted lines represent the LSWT result. In agreement with Refs. 6 and 16,  $P^{+-}(\mathbf{k})$  is decreased with respect to the LSWT result. Mainly responsible for this reduction is the first-order correction, which renormalizes the one-magnon peak by a factor  $D = 0.60684$ , whereas the second-order correction increases the integrated intensity by the contribution of the three-magnon sideband.

The results in Figs. 5 and 6 are qualitatively very similar to the ones obtained by Singh by series expansion.<sup>16</sup> We estimate

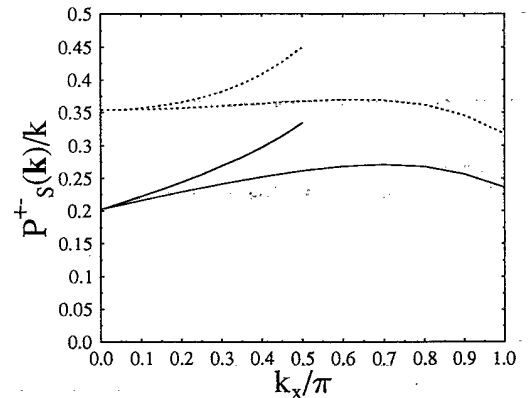


FIG. 5. Plot of  $P_S^{+-}(\mathbf{k})/k$  as a function of  $k_x$ , along the directions  $k_x = k_y$  and  $k_y = 0$  in momentum space. The dotted line is the LSWT approximation; the solid line is the second-order SWT. Note that in this case  $\mathbf{k}$  is restricted to the AFMBZ.

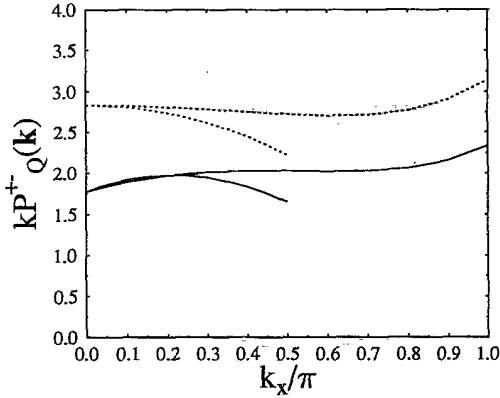


FIG. 6. Same as in Fig. 5 but for the quantity  $kP_Q^{+-}(\mathbf{k})$ .

$$\lim_{\mathbf{k} \rightarrow 0} P_S^{+-}(\mathbf{k})/k \approx 2 \times 0.10133, \quad (3.27)$$

$$\lim_{\mathbf{k} \rightarrow 0} kP_Q^{+-}(\mathbf{k}) \approx 2 \times 0.9288, \quad (3.28)$$

which should be compared with the series-expansion analysis by Singh:  $0.123 \pm 0.007$  and  $1.05 \pm 0.10$ . The factor of 2 here comes from our definition of the Fourier transform of the spin variables [see Eq. (2.17)], since we have divided the FT by  $1/\sqrt{N}$ , but the whole lattice has  $2N$  sites.

Another interesting quantity to compute is the first frequency moment of the transverse spectral density, defined as

$$\rho_1(\mathbf{k}) = \mathcal{F}(\mathbf{k})/P^{+-}(\mathbf{k}), \quad (3.29)$$

where

$$\begin{aligned} \mathcal{F}(\mathbf{k}) &\equiv \langle [S^+(\mathbf{k}), H] S^-(\mathbf{k}) \rangle \\ &= \langle S^+(\mathbf{k}) (H - E_0) S^-(\mathbf{k}) \rangle \\ &= \int_{-\infty}^{+\infty} d\omega \omega P^{+-}(\mathbf{k}, \omega). \end{aligned} \quad (3.30)$$

Here  $E_0$  is the ground-state energy and the square brackets stand for the quantum commutator. The first moment is an estimate of the average excitation energy of all modes contributing to the spectral function at a given  $\mathbf{k}$ . Equation (3.30) is also known as a single-mode approximation (SMA),<sup>26</sup> because it can be interpreted as if there is a single mode which saturates 100% of the “oscillator strength,”  $\mathcal{F}(\mathbf{k})$ . In this sense  $\rho_1(\mathbf{k})$  is a variational estimate of the spin-wave energy at a given  $\mathbf{k}$ . The SMA is equivalent to assuming that the variational wave function  $S^+(\mathbf{k})|\psi\rangle$ , where  $|\psi\rangle$  is the exact ground state for  $H$ , is an exact eigenfunction corresponding to a “spin-wave” excited state at wave vector  $\mathbf{k}$ .<sup>26</sup> In Fig. 7 we have plotted the LSWT magnon dispersion  $\epsilon_{\mathbf{k}}$ , the second-order magnon dispersion  $\epsilon^{(2)}(\mathbf{k}) = \alpha(S)[\epsilon_{\mathbf{k}} + \tilde{\Sigma}_{\alpha\alpha}(\mathbf{k}, \epsilon_{\mathbf{k}})]$ , and the SMA dispersion  $\epsilon_{\text{SMA}}(\mathbf{k}) = \rho_1(\mathbf{k})/(JSz)$  (here the energies are measured in units of  $JSz$ ) as a function of  $\mathbf{k}$ , along the  $k_x = k_y$  direction in momentum space, for  $S = 1/2$ .  $\epsilon^{(2)}(\mathbf{k})$  was studied in detail in Ref. 7, where we showed that it is roughly proportional to  $\epsilon_{\mathbf{k}}$

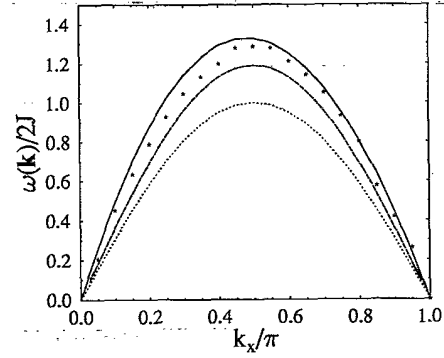


FIG. 7. Various “spin-wave” dispersions: The dotted line is the SWT magnon dispersion in the linear approximation. The dashed line is the SWT magnon dispersion corrected by the second-order self-energy. The solid line is the spin-wave dispersion obtained from the SWT transverse structure factor and the SMA. The stars represent the same SMA dispersion obtained by series expansion in Ref. 16. The dispersion is in units of  $2J$ .

over the entire AFBZ, with a renormalization constant  $Z_{\text{SW}}^{(2)}(\mathbf{k}) = \epsilon^{(2)}(\mathbf{k})/\epsilon(\mathbf{k})$  which varies smoothly between 1.18 and 1.20. This one-magnon dispersion is in excellent agreement with the dispersion obtained in recent experiments in  $\text{La}_2\text{CuO}_4$ .<sup>27</sup> The SMA dispersion  $\epsilon_{\text{SMA}}(\mathbf{k})$  behaves in a similar way and, in particular, it vanishes linearly at  $k = 0$  and  $k = (\pi, \pi)$ . The stars in the plot are the SMA dispersion derived by Singh by series expansion.<sup>16</sup> The agreement between the two SMA dispersions is good for  $k_x$  between  $\pi/2$  and  $\pi$  (corresponding to the staggered part of the correlation function), but worse in the region of  $k_x$  between 0 and  $\pi/2$ . Note that  $\epsilon_{\text{SMA}}(\mathbf{k})$  derived by series expansion drops slightly downward at  $k_x \approx 0.4\pi$ . For a more quantitative comparison of the SMA and magnon dispersions, we introduce the renormalization constant with respect to  $\epsilon_{\mathbf{k}}$ ,  $Z_{\text{SMA}}(\mathbf{k}) = \epsilon_{\text{SMA}}(\mathbf{k})/\epsilon_{\mathbf{k}}$ . The renormalization constants  $Z_{\text{SW}}^{(2)}(\mathbf{k})$  and  $Z_{\text{SMA}}(\mathbf{k})$  are plotted in Fig. 8, where the  $Z_{\text{SMA}}(\mathbf{k})$  calculated by Singh by series expansion is also

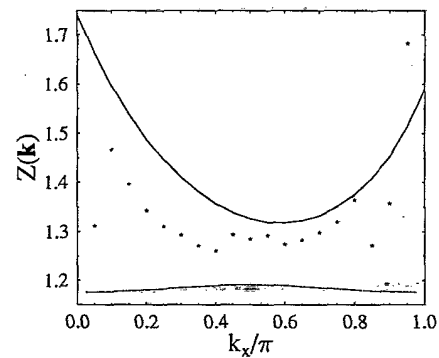


FIG. 8. Dispersion renormalization constant defined as the ratio of the spin-wave dispersion to the LSWT dispersion. The dashed line is from the second-order magnon dispersion. The solid line is from the SMA approximation. The stars are from the SMA of Ref. 16.

reported. Near the zone center and the antiferromagnetic wave vector, the series-expansion renormalization seems to fluctuate considerably. The corresponding SW result is smoother, but it becomes rather large in these two limits. In fact, we estimate

$$\lim_{\mathbf{k} \rightarrow 0} Z_{\text{SMA}}(\mathbf{k}) = 1.7401 \pm 0.0007, \quad (3.31a)$$

$$\lim_{\mathbf{k} \rightarrow (\pi, \pi)} Z_{\text{SMA}}(\mathbf{k}) = 1.5897 \pm 0.0006. \quad (3.31b)$$

In Ref. 16 the limit behavior of the SMA dispersion at  $\mathbf{k} = 0$  and  $\mathbf{k} = (\pi, \pi)$  is estimated indirectly by extrapolating from the middle of the zone the quantities plotted in Figs. 5 and 6. The result obtained there is

$$\lim_{\mathbf{k} \rightarrow 0} Z_{\text{SMA}}(\mathbf{k}) = 1.45 \pm 0.10, \quad (3.31c)$$

$$\lim_{\mathbf{k} \rightarrow (\pi, \pi)} Z_{\text{SMA}}(\mathbf{k}) = 1.36 \pm 0.13. \quad (3.31d)$$

The series-expansion estimate should be considered more accurate, and we do not understand why the spin-wave expansion is less effective than usual here. The ratio of  $Z_{\text{SW}}(\mathbf{k})$  to  $Z_{\text{SMA}}(\mathbf{k})$  is a quantitative measure of the fraction of multiple-magnon excitations present in the transverse spectral function, due to the nonlinearities of the spin-wave formalism. Apart from the regions near the zone center and near the antiferromagnetic vector, our results imply that throughout the LBZ this fraction is about 10–15% of the total. This is in agreement with the series-expansion result and thus further strengthens the validity of spin-wave theory.

### C. Transverse susceptibility

In this section we compute the second-order correction to the transverse static uniform susceptibility. The transverse or perpendicular susceptibility is the quantity that measures the response of the system to an external magnetic field, applied in a direction perpendicular to the staggered magnetization. Suppose that we add to the Hamiltonian (2.1) a term of the form  $H_{\perp} \sum_l S_l^z$ . The perpendicular susceptibility is defined as  $\chi_{\perp} \equiv \partial \langle M_{\perp} \rangle / \partial H_{\perp}$ , where  $\langle M_{\perp} \rangle$  is the ground-state expectation value of  $\frac{1}{2N} \sum_l S_l^z$ . In linear-response theory we can relate  $\chi_{\perp}$  to the transverse uniform Green's function studied before. One can see that

$$\chi_{\perp} = -\frac{1}{4} \lim_{\mathbf{k} \rightarrow 0} \lim_{\omega \rightarrow 0} \mathcal{P}_S^{+-}(\mathbf{k}, \omega). \quad (3.32)$$

The LSW result is easily obtained:

$$\chi_{\perp}^{(0)} = 1/2zJ. \quad (3.33)$$

We express the higher-order corrections in terms of a renormalization constant defined as

$$Z_{\chi} \equiv \frac{\chi_{\perp}}{\chi_{\perp}^{(0)}}, \quad (3.34)$$

which is then expanded in perturbation theory. To get

the result to second order, we put the second-order expressions of  $F_{\mu\nu}(\mathbf{k}, \omega = 0)$ , given by Eq. (3.14), into Eq. (3.5), and take the  $k \rightarrow 0$  limit, remembering that  $u_{\mathbf{k}}^2(1 - x_{\mathbf{k}})^2 \rightarrow \epsilon_{\mathbf{k}}/2$  in this limit. We obtain

$$Z_{\chi} = \frac{1}{\alpha(S)} \left[ D - D(\tilde{\sigma}_{\alpha\alpha} + \tilde{\sigma}_{\alpha\beta}) + \tilde{i}_{\alpha\alpha} + \tilde{i}_{\alpha\beta} \right], \quad (3.35)$$

where

$$\tilde{\sigma}_{\mu\nu} = \lim_{\mathbf{k} \rightarrow 0} \frac{\tilde{\Sigma}_{\mu\nu}(\mathbf{k}, 0)}{\epsilon_{\mathbf{k}}}, \quad (3.36)$$

$$\tilde{i}_{\mu\nu} = \lim_{\mathbf{k} \rightarrow 0} \frac{\tilde{I}_{\mu\nu}(\mathbf{k}, 0)}{\epsilon_{\mathbf{k}}}, \quad (3.37)$$

and we have used the equalities

$$\tilde{\sigma}_{\alpha\alpha} = \tilde{\sigma}_{\beta\beta}, \quad (3.38a)$$

$$\tilde{\sigma}_{\beta\alpha} = \tilde{\sigma}_{\alpha\beta}, \quad (3.38b)$$

$$\tilde{i}_{\alpha\alpha} = \tilde{i}_{\beta\beta}, \quad (3.38c)$$

$$\tilde{i}_{\beta\alpha} = \tilde{i}_{\alpha\beta}. \quad (3.38d)$$

We have evaluated  $\tilde{\sigma}_{\alpha\alpha}$ ,  $\tilde{\sigma}_{\alpha\beta}$ ,  $\tilde{i}_{\alpha\alpha}$ ,  $\tilde{i}_{\alpha\beta}$  by Monte Carlo integration. Near the origin these quantities are almost  $\mathbf{k}$  independent.

In order to obtain a  $1/S$  series of  $Z_{\chi}$ , we need to expand all the quantities and constants in Eq. (3.35) in powers of  $1/S$ . We obtain

$$Z_{\chi} = 1 - \frac{0.551148}{(2S)} + \frac{0.023194 \pm 0.00039}{(2S)^2} + \mathcal{O}(1/2S)^3. \quad (3.39)$$

For  $S = 1/2$ , the second-order correction increases the value of  $Z_{\chi}$  from 0.4488 to  $0.47204 \pm 0.00039$ , improving the agreement with the series-expansion results,<sup>3,28</sup> which gives  $\approx 0.52$ . Note that we do not expand Eq. (3.35) in  $1/S$ ; the result is somewhat closer to the series-expansion estimate, which is  $Z_{\chi} = 0.48443 \pm 0.00010$ . However, the second-order correction in Eq. (3.39) is smaller than  $0.0544/(2S)^2$  obtained by Hamer, Zheng, and Arndt<sup>28</sup> and also smaller than  $0.065/(2S)^2$  obtained by Igarashi.<sup>25</sup> We have so far not been able to find the reason for the discrepancy. Note that in both these two works the umklapp phases seem to have been treated correctly.

## IV. LONGITUDINAL CORRELATION FUNCTION

In this section we study the longitudinal correlation function.

We start by rewriting  $S^z(\mathbf{k})$  and  $Q^z(\mathbf{k})$  in the following form:

$$S^z(\mathbf{k}) = \frac{1}{\sqrt{N}} \sum_{12} \delta_{\mathbf{G}} \left[ f_1^-(1,2)(\alpha_1^\dagger \alpha_2 - \phi_{\mathbf{G}} \beta_2^\dagger \beta_1) \right. \\ \left. + f_2^-(1,2)(\alpha_1^\dagger \beta_2^\dagger - \phi_{\mathbf{G}} \alpha_2 \beta_1) \right],$$

$$Q^z(\mathbf{k}) = \sqrt{N} 2SD \delta(\mathbf{k}) \\ - \frac{1}{\sqrt{N}} \sum_{12} \delta_{\mathbf{G}} \left[ f_1^+(1,2)(\alpha_1^\dagger \alpha_2 + \phi_{\mathbf{G}} \beta_2^\dagger \beta_1) \right. \\ \left. + f_2^+(1,2)(\alpha_1^\dagger \beta_2^\dagger + \phi_{\mathbf{G}} \alpha_2 \beta_1) \right], \quad (4.1)$$

where we have introduced the functions

$$f_1^+(1,2) = \phi_{\mathbf{G}} v_1 v_2 + u_1 u_2, \quad (4.2a)$$

$$f_1^-(1,2) = \phi_{\mathbf{G}} v_1 v_2 - u_1 u_2, \quad (4.2b)$$

$$f_2^+(1,2) = \phi_{\mathbf{G}} v_1 u_2 + u_1 v_2, \quad (4.2c)$$

$$f_2^-(1,2) = \phi_{\mathbf{G}} v_1 u_2 - u_1 v_2, \quad (4.2d)$$

and

$$v_{\mathbf{k}} = -u_{\mathbf{k}} x_{\mathbf{k}}.$$

When we use Eqs. (4.1) and (4.1) in Eqs. (2.31) and (2.32), we obtain lengthy expressions involving up to 16 two-particle Green's function, which can be reduced to eight by symmetry properties under  $\alpha^\dagger \rightarrow \beta$ . However, it is easy to see that to get the same order of approximation in  $1/zS$  that we got for the transverse correlation function, we need to expand these two-particle Green's functions to first order in perturbation theory. It turns out that, to first order, only 3 of the 16 contribute. We arrive at the following equations for the longitudinal spectral functions  $L_S(\mathbf{k}, \omega)$  and  $L_Q(\mathbf{k}, \omega)$ :

$$L_S(\mathbf{k}, \omega) = -\frac{1}{\pi} \text{Im} \mathcal{L}_S(\mathbf{k}, \omega) \\ = \frac{1}{N} \sum_{1234} \delta_{\mathbf{G}_1}(1-2-\mathbf{k}) \delta_{\mathbf{G}_2}(3-4+\mathbf{k}) f_2^-(1,2) f_2^-(3,4) \\ \times \left( -\frac{1}{\pi} \right) \text{Im} \left[ -\phi_{\mathbf{G}_1} \Pi(\omega) + \chi_a(\omega) + \phi_{\mathbf{G}_1} \phi_{\mathbf{G}_2} \chi_b(\omega) \right], \quad (4.3)$$

$$L_Q(\mathbf{k}, \omega) = -\frac{1}{\pi} \text{Im} \mathcal{L}_Q(\mathbf{k}, \omega) = 8NSD(SD - 2\delta S) \delta(\omega) \delta(\mathbf{k}) \\ + \frac{1}{N} \sum_{1234} \delta_{\mathbf{G}_1}(1-2-\mathbf{k}) \delta_{\mathbf{G}_2}(3-4+\mathbf{k}) f_2^+(1,2) f_2^+(3,4) \\ \times \left( -\frac{1}{\pi} \right) \text{Im} \left[ \phi_{\mathbf{G}_1} \Pi(\omega) + \chi_a(\omega) + \phi_{\mathbf{G}_1} \phi_{\mathbf{G}_2} \chi_b(\omega) \right], \quad (4.4)$$

where  $\Pi(\omega)$ ,  $\chi_a(\omega)$ , and  $\chi_b(\omega)$  are two-particle Green's functions defined as

$$\Pi(t) = -i \langle T \beta_1(t) \alpha_2(t) \alpha_3^\dagger(0) \beta_4^\dagger(0) \rangle, \quad (4.5)$$

$$\chi_a(t) = -i \langle T \alpha_1^\dagger(t) \beta_2^\dagger(t) \beta_4^\dagger(0) \alpha_3^\dagger(0) \rangle, \quad (4.6)$$

$$\chi_b(t) = -i \langle T \beta_1(t) \alpha_2(t) \alpha_4(0) \beta_3(0) \rangle. \quad (4.7)$$

The constant  $\delta S$  is given by

$$\delta S = \frac{1}{N} \sum_{\mathbf{k}} u_{\mathbf{k}}^2 \left[ \frac{(1+x_{\mathbf{k}}^2)}{2} (\langle \alpha_{\mathbf{k}}^\dagger \alpha_{\mathbf{k}} \rangle + \langle \beta_{\mathbf{k}}^\dagger \beta_{\mathbf{k}} \rangle) \right. \\ \left. - x_{\mathbf{k}} (\langle \alpha_{\mathbf{k}}^\dagger \beta_{\mathbf{k}}^\dagger \rangle + \langle \alpha_{\mathbf{k}} \beta_{\mathbf{k}} \rangle) \right] \quad (4.8)$$

and can be calculated using the expressions for the one-particle Green's function derived in Sec. III. It turns out that the leading order and the first order are identically zero. The second-order correction can be shown to be equal to the second-order correction of the spin reduction of the staggered magnetization. The spin reduction is defined as  $\Delta S = S - \langle S_i^z \rangle$ . We have previously obtained the second-order correction<sup>14</sup>

$$\delta S^{(2)} = \Delta S^{(2)} = (-0.00354 \pm 0.00020) 2S. \quad (4.9)$$

Therefore the staggered magnetization to second order is

$$m \equiv \langle S_i^z \rangle = S - 0.196660(2S)^0 + 0 \times (2S)^{-1} \\ + 0.00354(2S)^{-2}. \quad (4.10)$$

This value for the second-order spin-wave correction to the staggered magnetization has also been obtained recently by Igarashi<sup>25</sup> using the HP formalism and by Hamer, Zheng, and Arndt<sup>28</sup> using both the HP and DM formalisms. It disagrees with the results obtained in an earlier paper by Igarashi and Watabe<sup>6</sup> and by Castilla and Chakravarty,<sup>8</sup> where umklapp processes were not treated correctly. For  $S = 1/2$ , Eq. (4.10) gives  $m = 0.3069 \pm 0.00020$ , improving the agreement with the best series-expansion estimate  $m = 0.307 \pm 0.002$ .<sup>29,3</sup>

We now come to the perturbation analysis of the three two-particle correlation functions defined above. To leading order it is obvious that only  $\Pi(\omega)$  contributes through the process shown in Fig. 9(a), describing two noninter-

acting magnons of momentum  $\mathbf{k}_1$  and  $\mathbf{k}_2 + \mathbf{k} + \mathbf{G}$ . The imaginary part is

$$-\frac{1}{\pi} \text{Im} \Pi^{(0)}(\omega) = \frac{1}{\Omega_{\max}} \delta_{1,4} \delta_{2,3} \delta(\tilde{\omega} - \epsilon_1 - \epsilon_2). \quad (4.11)$$

To first order each of the three Green's function has a contribution, shown in Figs. 9(b)–9(d). While the first-order correction to  $\Pi$  clearly describes two magnons interacting once, the other two graphs have a less transparent meaning. Their imaginary part for  $\omega > 0$  is

$$\left(-\frac{1}{\pi}\right) \text{Im} \Pi^{(1)}(\omega) = -\frac{1}{\Omega_{\max} 4\alpha(S)S} \frac{1}{N} V_{2431}^{(4)} \frac{\delta(\omega - \epsilon_1 - \epsilon_2) - \delta(\omega - \epsilon_3 - \epsilon_4)}{\epsilon_1 + \epsilon_2 - \epsilon_3 - \epsilon_4}, \quad (4.12)$$

$$\left(-\frac{1}{\pi}\right) \text{Im} \chi_a^{(1)}(\omega) = \frac{4}{\Omega_{\max} 4\alpha(S)S} \frac{1}{N} V_{2431}^{(8)} \frac{\delta(\omega - \epsilon_3 - \epsilon_4)}{\epsilon_1 + \epsilon_2 + \epsilon_3 + \epsilon_4}, \quad (4.13)$$

$$\left(-\frac{1}{\pi}\right) \text{Im} \chi_b^{(1)}(\omega) = \frac{4}{\Omega_{\max} 4\alpha(S)S} \frac{1}{N} V_{2431}^{(7)} \frac{\delta(\omega - \epsilon_1 - \epsilon_2)}{\epsilon_1 + \epsilon_2 + \epsilon_3 + \epsilon_4}. \quad (4.14)$$

We then use Eqs. (4.12)–(4.14) in Eqs. (4.4) and (4.3), and sum over the momenta. The first-order correction to  $\Pi(\omega)$  is not easy to evaluate because the factor  $1/(\epsilon_1 + \epsilon_2 - \epsilon_3 - \epsilon_4)$  causes convergence problems. However, we see that the integrated intensity (integral over all the frequencies) of this term is identically zero. This “sum rule” can be effectively used to control a regularization parameter that we must introduce to get reasonable convergence. The final result for the longitudinal spectral function is plotted in Figs. 10 and 11 for several values of the momentum  $\mathbf{k}$ . The noninteracting line shapes (dotted lines) display a double-peak structure, except for the staggered part at  $\mathbf{k} = \mathbf{0}$ , which has the expected elastic peak at  $\omega = 0$ . The first of these two  $\delta$ -function peaks occurs at the one-magnon frequency  $\omega = \Omega_{\max} \epsilon_{\mathbf{k}}$ , while the second peak, located between  $\Omega_{\max} \epsilon_{\mathbf{k}}$  and  $2\Omega_{\max}$ , is a two-magnon resonance with total momentum  $\mathbf{k}$ . Note that the two-magnon peak is more intense than the one-magnon peak. We also want to emphasize that again the umklapp phases affect the line shape even qualitatively. If we neglect them, by setting  $\phi_{\mathbf{G}} = 1$ , the second peak is completely washed out. This noninteracting longitudinal line shape is remarkably close to the Schwinger-boson mean-field (SBMF) result of Auerbach and Arovas.<sup>30</sup> We

refer particularly to a paper by Chen and Shuttler<sup>31</sup> where the SBF structure factor was compared to exact results. The SBF line shape for the structure factor for  $T \rightarrow 0$  has also two peaks located exactly at the same position of our spin-wave result, with the difference that in the SBF case the first peak is higher than the second. This is interesting because it shows that in the  $T \rightarrow 0$  limit the SBF formalism, which is rotational invariant, exactly reproduces the situation of spin-wave theory, where a putative ordered state is assumed *a priori*.

When the magnon interaction is considered to first order, the longitudinal structure factor is modified in the way shown in Figs. 10 and 11 by the solid curves. It turns out that the first-order correction coming from  $\Pi(\omega)$  is rather small and simply tends to redistribute the spectral weight to lower frequencies by moving down the two-magnon peak. This is similar to what happens in a more dramatic way in two-magnon Raman scattering,<sup>13</sup> where the magnon interaction, which is essentially attractive, tends to form a lower-energy bound state. The first-order contribution coming from  $\chi_a(\omega)$  and  $\chi_b(\omega)$  is negative for all the frequencies, with a peak at the two-magnon energy. For some wave vectors this negative contribution is large enough to suppress substantially the two-magnon peak, in agreement with the suggestion of Auerbach and Arovas<sup>30</sup> that the gap between the two peaks is an artifact of the mean-field approximation. However, for other wave vectors [see in particular Fig. 10(c) for the wave vector  $\mathbf{k} = (\pi/2, \pi/2)$ ] the two-magnon peak, although reduced, seems to be robust against the interaction. Moving towards the antiferromagnetic wave vector, the two-magnon peak becomes in fact the dominant peak even with the first-order correction [see Fig. 11(c)] and eventually merges with the one-magnon peak to give the elastic peak at  $\omega = 0$ ,  $\mathbf{k} = (\pi, \pi)$ .

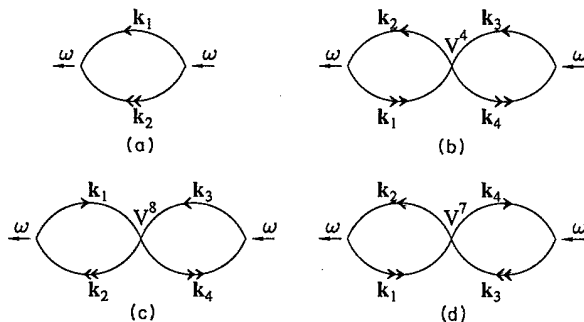


FIG. 9. Diagrams contributing to the two-particle Green's functions  $\Pi$ ,  $\chi_a$ , and  $\chi_b$  to first order. (a) Noninteracting (zeroth-order) contribution to  $\Pi$ . (b) First-order correction to  $\Pi$ . (c) First-order correction to  $\chi_a$ . (d) First-order correction to  $\chi_b$ .

## V. CONCLUSIONS

In this paper we have studied the spin-spin correlation function of the two-dimensional Heisenberg model

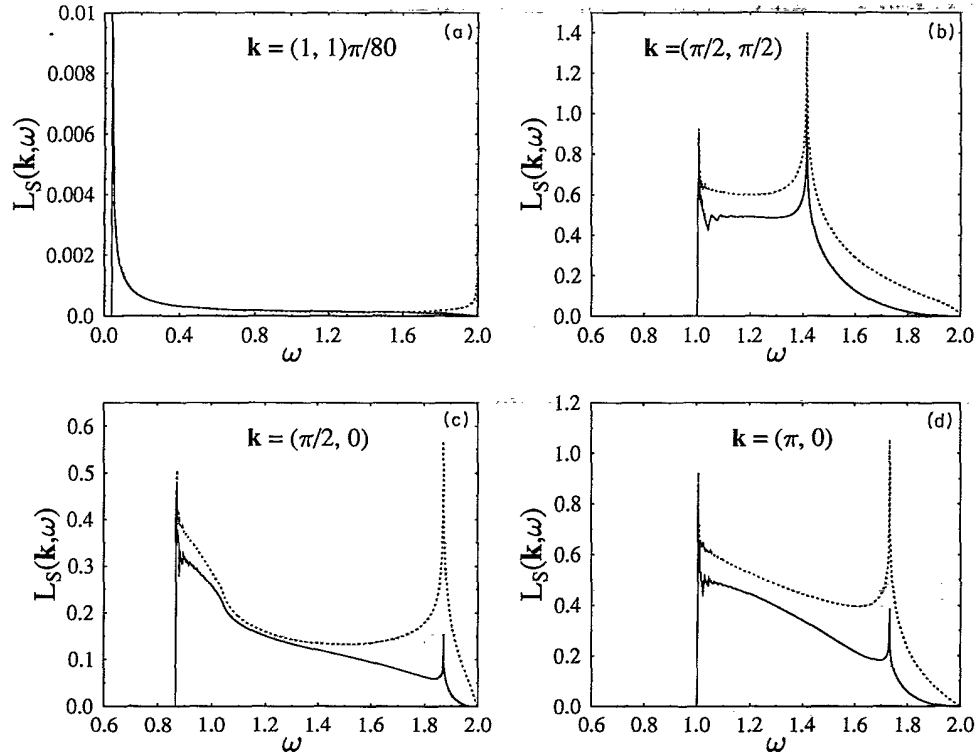


FIG. 10. Dynamical longitudinal uniform structure factor as a function of the frequency (in units of  $\Omega_{\max}$ ) for several values of the wave vector  $\mathbf{k}$ . The dotted line is the noninteracting approximation. The solid line is the interacting case to first order.

at  $T = 0$  by using the Dyson-Maleev spin-wave theory. We find that the dynamical transverse structure factor to second order in perturbation theory is characterized by a  $\delta$ -function peak at the one-magnon excitation energy (which is a threshold for the spectral density) and by a continuum at higher energies due to

three-magnon excitations. The relative intensity of the three-magnon sideband to the one-magnon peak is very small (about 1%) for wave vectors near the zone center and the antiferromagnetic wave vector, but it becomes a non-negligible fraction (about 20%) near the boundaries of the AFMBZ. The amount of three-magnon exci-

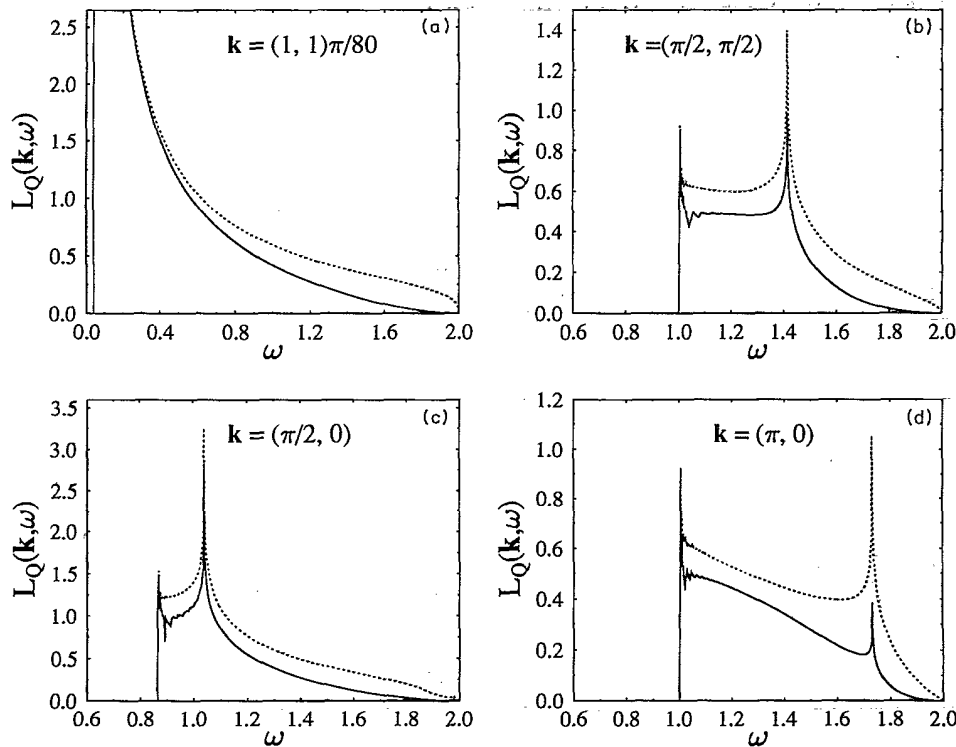


FIG. 11. Dynamical longitudinal staggered structure factor as a function of the frequency (in units of  $\Omega_{\max}$ ) for several values of the wave vector  $\mathbf{k}$ . The dotted line is the noninteracting approximation. The solid line is the interacting case to first order. For wave vectors on the AFMBZ boundary [see (b) and (d)], the staggered part is equivalent to the uniform part.

tations is, however, considerably smaller than what obtained in Ref. 6. In contrast to Ref. 6 we have carefully included the umklapp processes which are important in the calculations of the second-order corrections and are, most likely, the reason of our different results. However, we do not exclude that the DM formalism behaves differently from the HP formalism used in Ref. 6 for this kind of calculation. We have compared our results for the transverse equal-time correlations with recent series-expansion estimates,<sup>16</sup> finding good qualitative and quantitative agreement. In particular, we have evaluated the first frequency moment of the correlation function which gives an estimate of the spin-wave dispersion in the SMA. As in Ref. 16 we have found linear gapless modes near  $\mathbf{k} = 0$  and  $\mathbf{k} = (\pi, \pi)$ . The SMA dispersion is approximately  $1.4 \pm 0.1$  times the linear spin-wave dispersion throughout the BZ, in agreement with Ref. 16, except near  $\mathbf{k} = 0$  and  $\mathbf{k} = (\pi, \pi)$ , where it is larger than 1.5. Note that near these two points the SMA dispersion derived by series expansion fluctuates considerably. This renormalization factor is a about 10% bigger than the renormalization factor of the magnon dispersion, corrected by the second-order self-energy, and is a quantitative estimate of the mixing of three magnons. Our results and the comparison with the series-expansion calculations strengthen further the validity of spin-wave theory and show that the contribution of multiple-magnon excitations, although detectable, is always rather small and does not change substantially the picture derived from the (renormalized) linear spin-wave theory. New and more refined neutron-scattering experiments at higher energies will be very important to clarify the exact contribution of the multiple-magnon excitations in the structure factor.

We have also studied the longitudinal structure factor, which is nontrivial even in the spin-wave broken-symmetry ground state, because of the presence of quantum fluctuations. The leading-order approximation, involving two noninteracting magnons, displays a line shape identical to the one obtained by the Schwinger-boson formalism.<sup>30,31</sup> It is characterized by a  $\delta$ -function peak at the one-magnon frequency  $\epsilon_{\mathbf{k}}$  and by a sharp resonance at higher energies, identified as a two-magnon excitation. Magnon interaction to first order suppresses considerably the intensity of the two-magnon peak, except near the antiferromagnetic wave vector, where this peak remains the dominant excitation and eventually merges with the one-magnon peak to give the expected elastic peak at  $(\pi, \pi)$ . For wave vectors on the AFMBZ boundary, along the  $k_x = k_y$  direction in momentum space, the two peaks remain stable, with comparable weight, even after including the interaction. These results might be checked experimentally.

Finally we have computed the second-order correction to the staggered magnetization and to the renormalization constant of the perpendicular static susceptibility, improving further the agreement between the SW results and the series-expansion estimates of these quantities.

#### ACKNOWLEDGMENTS

We would like to thank S. M. Girvin for discussions and encouragement. We are very grateful to R. R. P. Singh for communicating his results before publication. One of us (C.M.C.) would also like to thank W. Stephan for discussions. M.W. is supported by the Swedish Natural Science Research Council, the Swedish National Board for Industrial and Technical Development, and NCSA.

### APPENDIX

#### 1. Second-order self-energy

$$\begin{aligned} \Sigma_{\alpha\alpha}^{(2)}(\mathbf{k}, \omega) &= \Sigma_{\beta\beta}^{(2)}(\mathbf{k}, -\omega) \\ &= \Omega_{\max} \frac{1}{[2\alpha(S)]^2 (2S)^2 N^2} \sum_{234} \delta_{\mathbf{G}}(\mathbf{k} + 2 - 3 - 4) \\ &\quad \times \left[ \frac{2V_{\mathbf{k}234}^{(2)} V_{432\mathbf{k}}^{(3)}}{\tilde{\omega} - \epsilon_2 - \epsilon_3 - \epsilon_4 + i\eta} - \frac{8V_{\mathbf{k}234}^{(7)} V_{432\mathbf{k}}^{(8)}}{\tilde{\omega} + \epsilon_2 + \epsilon_3 + \epsilon_4 - i\eta} \right], \end{aligned} \quad (\text{A1})$$

$$\begin{aligned} \Sigma_{\alpha\beta}^{(2)}(\mathbf{k}, \omega) &= \Sigma_{\beta\alpha}^{(2)}(\mathbf{k}, -\omega) \\ &= \Omega_{\max} \frac{1}{[\alpha(S)]^2 (2S)^2 N^2} \sum_{234} \delta_{\mathbf{G}}(\mathbf{k} + 2 - 3 - 4) \\ &\quad \times \left[ \frac{V_{\mathbf{k}234}^{(7)} V_{432\mathbf{k}}^{(5)}}{\tilde{\omega} + \epsilon_2 + \epsilon_3 + \epsilon_4 - i\eta} - \frac{V_{\mathbf{k}234}^{(2)} V_{432\mathbf{k}}^{(7)}}{\tilde{\omega} - \epsilon_2 - \epsilon_3 - \epsilon_4 + i\eta} \right]. \end{aligned} \quad (\text{A2})$$

2. Functions  $I_{\mu\nu}$ 

$$I_{\alpha\alpha}^{(2)}(\mathbf{k}, \omega) = \frac{1}{\alpha(S)(2S)^2} \frac{1}{N^2} \sum_{234} \delta_{\mathbf{G}}(\mathbf{k} + 2 - 3 - 4) u_{\mathbf{k}} u_2 u_3 u_4 \\ \times \left[ \frac{M_{\mathbf{k}234}^{(1)} V_{342\mathbf{k}}^{(3)}}{\tilde{\omega} - \epsilon_2 - \epsilon_3 - \epsilon_4 + i\eta} - \frac{2M_{\mathbf{k}234}^{(2)} V_{342\mathbf{k}}^{(8)}}{\tilde{\omega} + \epsilon_2 + \epsilon_3 + \epsilon_4 - i\eta} \right], \quad (\text{A3})$$

$$I_{\beta\beta}^{(2)}(\mathbf{k}, \omega) = \frac{1}{\alpha(S)(2S)^2} \frac{1}{N^2} \sum_{234} \delta_{\mathbf{G}}(\mathbf{k} + 2 - 3 - 4) \phi_{\mathbf{G}} u_{\mathbf{k}} u_2 u_3 u_4 \\ \times \left[ \frac{2M_{\mathbf{k}234}^{(2)} V_{342\mathbf{k}}^{(7)}}{\tilde{\omega} - \epsilon_2 - \epsilon_3 - \epsilon_4 + i\eta} - \frac{M_{\mathbf{k}234}^{(1)} V_{342\mathbf{k}}^{(5)}}{\tilde{\omega} + \epsilon_2 + \epsilon_3 + \epsilon_4 - i\eta} \right], \quad (\text{A4})$$

$$I_{\alpha\beta}^{(2)}(\mathbf{k}, \omega) = \frac{1}{\alpha(S)(2S)^2} \frac{1}{N^2} \sum_{234} \delta_{\mathbf{G}}(\mathbf{k} + 2 - 3 - 4) u_{\mathbf{k}} u_2 u_3 u_4 \\ \times \left[ \frac{2M_{\mathbf{k}234}^{(1)} V_{342\mathbf{k}}^{(7)}}{\tilde{\omega} - \epsilon_2 - \epsilon_3 - \epsilon_4 + i\eta} - \frac{M_{\mathbf{k}234}^{(2)} V_{342\mathbf{k}}^{(5)}}{\tilde{\omega} + \epsilon_2 + \epsilon_3 + \epsilon_4 - i\eta} \right], \quad (\text{A5})$$

$$I_{\beta\alpha}^{(2)}(\mathbf{k}, \omega) = \frac{1}{\alpha(S)(2S)^2} \frac{1}{N^2} \sum_{234} \delta_{\mathbf{G}}(\mathbf{k} + 2 - 3 - 4) \phi_{\mathbf{G}} u_{\mathbf{k}} u_2 u_3 u_4 \\ \times \left[ \frac{M_{\mathbf{k}234}^{(2)} V_{342\mathbf{k}}^{(3)}}{\tilde{\omega} - \epsilon_2 - \epsilon_3 - \epsilon_4 + i\eta} - \frac{2M_{\mathbf{k}234}^{(1)} V_{342\mathbf{k}}^{(8)}}{\tilde{\omega} + \epsilon_2 + \epsilon_3 + \epsilon_4 - i\eta} \right]. \quad (\text{A6})$$

- 
- <sup>1</sup> See, for example, S. Chakravarty, in *High Temperature Superconductivity Proceedings*, edited by K. S. Bedell *et al.* (Addison-Wesley, Redwood City, CA, 1990).
- <sup>2</sup> P. W. Anderson, *Phys. Rev.* **86**, 694 (1952); R. Kubo, *ibid.* **87**, 568 (1952).
- <sup>3</sup> R. R. P. Singh, *Phys. Rev. B* **39**, 9760 (1989).
- <sup>4</sup> J. D. Reger and A. P. Young, *Phys. Rev. B* **37**, 5979 (1988).
- <sup>5</sup> Zheng Weihong, J. Oitmaa, and C. J. Hamer, *Phys. Rev. B* **43**, 8321 (1991).
- <sup>6</sup> Jun-ichi Igarashi and Akihiro Watabe, *Phys. Rev. B* **43**, 13456 (1991).
- <sup>7</sup> C. M. Canali, S. M. Girvin, and Mats Wallin, *Phys. Rev. B* **45**, 10131 (1992).
- <sup>8</sup> G. E. Castilla and S. Chakravarty, *Phys. Rev. B* **43**, 13 687 (1991).
- <sup>9</sup> Jinsuk Song and James F. Arnett, *Phys. Rev. B* **42**, 4208 (1990).
- <sup>10</sup> K. B. Lyons *et al.*, *Phys. Rev. B* **37**, 2353 (1988).
- <sup>11</sup> J. B. Parkinson, *J. Phys. C* **2**, 2012 (1968).
- <sup>12</sup> R. R. P. Singh, *Phys. Rev. B* **41**, 4873 (1990).
- <sup>13</sup> C. M. Canali and S. M. Girvin, *Phys. Rev. B* **45**, 7127 (1992).
- <sup>14</sup> C. M. Canali, Ph.D. thesis, Indiana University, 1992.
- <sup>15</sup> S. W. Cheong *et al.*, *Phys. Rev. Lett.* **67**, 1791 (1991); G. Shirane *et al.*, *ibid.* **63**, 330 (1989); R. J. Birgenau *et al.*, *Phys. Rev. B* **38**, 6614 (1988).
- <sup>16</sup> R. R. P. Singh, *Phys. Rev. B* **47**, 12337 (1993).
- <sup>17</sup> F. J. Dyson, *Phys. Rev.* **102**, 1217 (1956); **102**, 1230 (1956).
- <sup>18</sup> S. V. Maleev, *Zh. Eksp. Theor. Fiz.* **30**, 1010 (1957) [*Sov. Phys. JETP* **64**, 654 (1958)].
- <sup>19</sup> C. M. Canali and S. M. Girvin, *Bull. Am. Phys. Soc.* **37**, 542 (1992).
- <sup>20</sup> P. Kopietz, *Phys. Rev. B* **41**, 9228 (1990).
- <sup>21</sup> A. B. Harris, D. Kumar, B. I. Halperin, and P. C. Hohenberg, *Phys. Rev. B* **3**, 961 (1971).
- <sup>22</sup> The second-order self-energy contains a factor  $[1/\alpha(S)]^2$ , coming from the Oguchi correction. When we say that the second-order self-energy is of order  $\mathcal{O}(1/S)$ , we mean that the *leading term*, obtained by expanding  $1/\alpha(S)$  in powers of  $1/S$ , is of order  $\mathcal{O}(1/S)$ .
- <sup>23</sup> A. Brooks Harris, *Phys. Rev. Lett.* **21**, 602 (1968).
- <sup>24</sup> M. G. Cottam and R. B. Stinchcombe, *J. Phys. C* **3**, 2283 (1970); **3**, 2305 (1970).
- <sup>25</sup> Jun-ichi Igarashi, *Phys. Rev. B* **46**, 10763 (1992).
- <sup>26</sup> R. P. Feynman, *Phys. Rev.* **94**, 262 (1954).
- <sup>27</sup> S. M. Hayden *et al.*, *Phys. Rev. Lett.* **67** 3622 (1991).
- <sup>28</sup> C. J. Hamer, Zheng Weihong, and Peter Arndt, *Phys. Rev. B* **46**, 6276 (1992); Zheng Weihong and C. J. Hamer (unpublished).
- <sup>29</sup> Zheng Weihong, J. Oitmaa, and C. J. Hamer, *Phys. Rev. B* **44**, 11869 (1991).
- <sup>30</sup> A. Auerbach and D. P. Arovas, *Phys. Rev. Lett.* **61**, 617 (1988).
- <sup>31</sup> C. X. Chen and H. B. Schutter, *Phys. Rev. B* **40**, 239 (1989).